PREDICTED AND FLIGHT DATA FOR AN 18 MM PISTON LAUNCHER

Research and Development Report

Prepared for: **NARCON-2017**
Herndon, Virginia
February 24-26, 2017

Submitted by: **Chris Flanigan**
NAR 17540 L1
C Division

ABSTRACT

This project had two objectives: 1) measure accelerations during piston phase of flight; and 2) compare flight results to analysis predictions. The project successfully achieved both objectives. The following activities were performed:

- Reviewed prior R&D reports related to piston launchers
- Performed new static testing of Estes C6 motors to provide high resolution thrust-vs-time curves
- Implemented the Piston Launcher Performance Program (originally developed by Geoff Landis) as an Excel spreadsheet
- Developed a test vehicle that included an altimeter/accelerometer to measure the axial accelerations during flight
- Performed flight testing for two mass configurations of the test vehicle launched using an 18 mm diameter piston launcher
- Used the PLPP spreadsheet to calculate responses for the test flight configurations
- Compared flight data to the analysis results

The analysis results were very sensitive to the representation of the thrust-time curve during the piston phase of flight. Using high resolution data from new static testing, the analysis results for vehicle accelerations and velocities had very good agreement to flight data. This showed that the piston launcher theory was accurate for size of piston launcher, motor, and model examined in this project. Future studies could examine other models and piston sizes.

Prepared by:

Christopher C. Flanigan
NAR 17540 L1

TABLE OF CONTENTS

NOMENCLATURE

γ	Adiabatic gas constant
A_p	Cross-section area of the piston tube
F	Force
F_g	Force caused by gravity
F_m	Force (thrust) from the rocket motor
F_p	Force caused by pressure inside the piston tube
g	Acceleration due to gravity
k_1	Rate of exhaust gas production (moles/N-sec)
L	Length
M	Mass
M_r	Mass of the rocket
M_p	Mass of the piston tube
P	Pressure
P_{atm}	Atmospheric pressure at the launch altitude
P_p	Pressure inside the piston tube
r_p	Radius of piston tube
R	Universal gas constant
T	Temperature
$T_{exhaust}$	Temperature of the motor exhaust gas
V	Volume
x	Displacement
$\dot{x}$	Velocity
$\ddot{x}$	Acceleration

ACRONYMS

FHPL	Floating head piston launcher
NAR	National Association of Rocketry
PLPP	Piston Launcher Performance Program

UNITS

G	Acceleration in gravities
K	Kelvin
m	Meters
N	Newtons

1 INTRODUCTION

Piston launchers are often used to improve the performance of competition models. A piston launcher captures the motor's exhaust gas inside a moving piston tube to increase vertical force during the piston's travel. Several design features control the piston's effectiveness including piston length, piston diameter, motor properties, and mass of the rocket.

Theoretical models describing the thermodynamic and physical operation of piston launchers have been published as early as 1972. However, the theoretical models have many assumptions that have not been thoroughly correlated to flight data.

Several prior R&D reports have published test and flight data (discussed further in Section 3 of this report). Historically, it has been difficult to obtain accurate and extensive flight data for piston launchers due many factors including 1) the time and effort required; 2) accuracy limitations of available instrumentation and measurement methods (photography, optical tracking, altimeters, etc.); 3) numerical ill-conditioning of data processing (calculating velocities and accelerations from displacements); and 4) the effects of other flight variables (vehicle drag, wind, etc.).

This project attempted to directly compare analysis predictions and flight data of a piston launcher during the piston phase of flight. Using modern electronics, the vehicle's acceleration during the piston phase of flight can be measured and compared to predictions. If the theoretical models of the piston operation can be calibrated and validated, then the theoretical models can be used with greater confidence to predict piston performance for a wide range of motors and vehicle designs.

This report describes the analysis approach, instrumentation methodology, flight measurements, and comparison of analysis and flight results.

2 OBJECTIVES AND APPROACH

2.1 OBJECTIVES

The objectives of this project were to 1) measure accelerations during piston phase of flight; and 2) compare flight results to analysis predictions. The comparison can be used to calibrate and validate the theoretical model. If the theoretical model can be validated, this will allow theory to be used to accurately predict performance for a wide range of motors and vehicle designs.

2.2 TECHNICAL APPROACH

The technical approach for this project was as follows:

- Review theory and flight data from prior R&D reports
- Perform static testing of motors to obtain higher resolution thrust-time data for the piston phase of flight
- Perform flight tests for selected configurations
- Calculate analysis predictions for the flight configurations
- Compare predictions and flight results

These steps are described in the following sections.

3 REVIEW OF PRIOR R&D REPORTS

Many R&D reports have been published describing piston launcher theory and flight results. Selected major reports are summarized below. See the R&D report archive on the NAR web site[1] for additional reports.

- **"An Investigation of the Dynamics of the Closed-Breech Launcher," The Barber Team (T-151), NARAM-14 R&D report, 1972**. Performed testing and analysis of closed breech launchers (large diameter launchers where the rocket fits inside the tube). Derived equations of motion for a pressurization launcher. Test data showed that large diameter pressure-assisted launchers did not provide additional performance when using 1/2A6 motors.
- **"Optimization of Zero-Volume Piston Launcher," R.Thoelen, T.Bauer, & P.Porzio, MITCON, 1973**. Results indicated that short piston lengths (7-10") were best.
- **"Investigation of the Physics of the Zero Volume Piston Launcher," Geoffrey Landis, NARAM-17 R&D report, 1975**. More detailed derivation of the theory for piston launchers. Included a FORTRAN computer program for calculating piston performance. Performed lab testing using strobe photography to measure piston displacement versus time.
- **"Floating Head Piston Launcher," Charles Weiss & Jeff Vincent, NARAM-28 R&D report, 1986**. Introduced the floating head piston launcher (FHPL) concept.
- **"Optimum Length for a Floating Head Piston Launcher," Charles Weiss & Jeff Vincent, NARAM-30 R&D report, 1988**. Results indicated that the optimum length for a FHPL was 7-9". Longer pistons did not provide additional performance.
- **"Piston Pressure and Massive Models," Robert & Peter Alway, NARAM-47 R&D report, 2005**. Results indicated that long pistons were better for "massive" models such as egglofters.
- **"Piston Effect on Thrust Curves," Patrick Peterson / Neutron Fusion Team, NARAM-55 R&D report, 2013**. Measured "piston-augmented thrust" by video of pistons moving in clear plastic tubes. Results indicated that long piston tubes are generally better. Optimum piston length may exceed 1.5 meters.

[1] http://www.nar.org/members/rd-reports-in-chronological-order

As noted above, some of the above R&D reports indicated that short piston tubes were best, while more recent reports found that long tubes were best. Additional work is needed to resolve this issue.

4 THEORY OF PISTON LAUNCHER OPERATION

Piston launcher operation is briefly summarized in Section 4.1. The thermodynamic and mechanical theory for piston launcher operation is provided in Section 4.2. Important assumptions are listed in Section 4.3.

4.1 PISTON LAUNCHER OVERVIEW

A typical floating head piston launcher is shown in Figure 4.1-1. The main components include:

- Support rod
- Piston head
- Piston tube including aft ring
- Rocket vehicle including motor

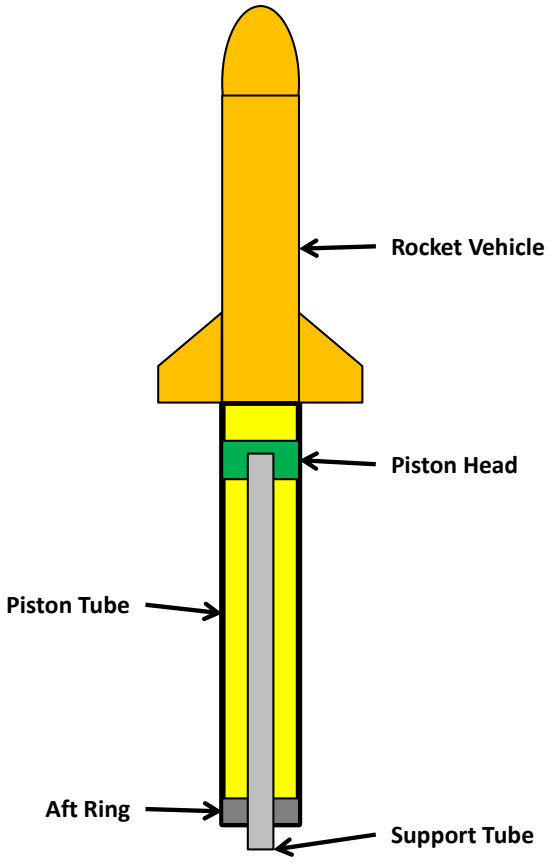

Figure 4.1-1. A piston launcher assembly includes a support tube, a moving piston tube with aft ring, a piston head, and the rocket vehicle (including motor).

The piston operation begins at an initial position with the rocket attached[2] to the top of the piston tube. The piston's initial volume[3] is filled with air at ambient temperature and pressure. After ignition, the motor produces exhaust gas which increases the pressure and temperature of the gas inside the piston. When the upwards pressure force from the piston exceeds the downwards gravity force on the rocket vehicle/piston tube assembly, the vehicle/tube assembly begins to move upwards. The vertical motion increases the piston volume, thereby affecting the internal pressure and temperature. The coupled interaction between the exhaust gas and piston/vehicle motion continues until the aft end of the piston reaches the piston head. At this point, the rocket vehicle detaches[4] from the piston tube and continues with the post-piston (unassisted) phase of flight.

4.2 THEORY

This section presents the description of piston launcher theory as presented by Landis [3].

Piston launchers act in accordance with several well-known laws of physics. Primary among these is Newton's second law of motion:

$$F = M\,\ddot{x} \tag{1}$$

[2] The rocket is typically connected to the piston tube by a friction fit. The friction fit must be tight enough to keep the piston tube attached to the rocket during the piston phase of flight. However, the friction fit must not be too tight so that the piston tube can be released/ejected immediately at the end of the piston phase of flight. Other methods for attachment have been used including mechanical arms or pins. The effects of rocket/tube release from the piston tube are not addressed in this report.

[3] Some prior R&D reports have implied that zero initial volume provides maximum piston performance. Other reports have implied that an initial zero volume produces oscillation in the piston motion that may degrade performance. An optimum value of the initial volume has not been conclusively demonstrated.

[4] For a classic "fixed head" piston launcher, the piston head attached to the support rod. For this design, the piston tube must come to an abrupt halt at the end of the piston travel. The rocket hopefully disconnects from the piston tube due to momentum and without excessive loss of energy (velocity). For a floating head piston launcher (FHPL), the piston head "floats" on the top of the support rod. At the end of the piston travel, the piston tube picks up the floating head, and both the piston tube and piston head depart from the support tube. Pressure increases rapidly in the piston tube until the piston tube and piston head are ejected from the rocket. Other release mechanisms have been used including mechanical arms and pull pins. As noted previously, the effects of rocket/tube release are not addressed in this report.

There are several forces acting on the rocket/piston tube assembly including gravity, thrust, internal pressure in the piston, aerodynamic drag, and friction. Gravity force depends on the mass of the rocket vehicle (including motor) and piston tube assembly:

$$F_g = \left(M_r + M_p\right) \mathrm{g} \tag{2}$$

where "g" is the acceleration due to gravity (9.80665 m/sec^2 at sea level).

The thrust produced by the motor depends on propellant properties and grain design. Static testing is performed by NAR Standards & Testing (S&T) to measure thrust versus time and related properties. For a piston launcher, the motor's thrust may be reduced slightly due to internal pressure in the piston.

The pressure force applied by the piston to the rocket is proportional to the piston diameter and the pressure inside the piston tube:

$$F_p = \pi {r_p}^2 \left(P_p - P_{atm}\right) \tag{3}$$

where P_{atm} = pressure of one atmosphere at sea level (101,325 N/m^2). The gas pressure inside the piston tube is assumed to follow the Ideal Gas Law:

$$P\,V = n\,R\,T \tag{4}$$

where

P = the pressure of the gas

V = the volume of the gas

n = the amount of substance of gas (in moles)

R = the ideal, or universal, gas constant, equal to the product of the Boltzmann constant and the Avogadro constant

T = the absolute temperature of the gas

T depends on the temperature of the motor's exhaust gas, which is nominally 1,500°K [10]. Several things affect temperature. First, when the exhaust gas mixes with the cooler gas already in the launcher, it will be cooled. The amount by which it is cooled is governed by the relative specific heats involved. A good approximation to the cooling due to mixing is:

$$T = (n\,T_{old} + \Delta n\,T_{exhaust})/(n + \Delta n) \quad (5)$$

The total temperature is the molewise average of the previous temperature in the piston and the temperature of the exhaust gas input.

n is a function of time determined by the motor thrust and impulse. For a motor of constant specific impulse, the rate of gas input is proportional to the thrust of the motor:

$$\frac{dn}{dt} = k_1 F_m(t) \quad (6)$$

where $F_m(t)$ is the motor's thrust as a function of time. Integrating the above equation:

$$n = k_1 \int_{t_0}^{t} F_m(t)dt \quad (7)$$

Note that the integral term in the above equation represents the impulse of the motor.

During the early part of the piston operation when pressure force is less than the gravity force on the rocket/tube assembly, the rocket /tube acceleration is set to zero so that the rocket/tube assembly remains at its initial location.

The volume in piston will produce a "gas spring" effect. The vibration frequency of the gas spring system can be calculated as[5]:

$$f_0 = \frac{1}{2\pi}\sqrt{\frac{\gamma\,P_{atm}\,A_p}{M\,L}}$$

where

f_0 = frequency (Hz)
γ = adiabatic gas constant
P_{atm} = atmospheric pressure [N/m^2]
A_p = cross-sectional area of air column [m^2]
L = length of air column [m]
M = mass supported on the air spring [kg]

[5] www.diracdelta.co.uk/science/source/a/i/air spring/source.html

The air spring frequency can provide insight into oscillations (if any) calculated during the piston phase of flight.

4.3 ASUMPTIONS

The theory for piston launcher operation presented in Section 4.2 includes many assumptions:

- Ideal gas law (neglect two-phase flow effects)
- Use published values for exhaust temperature and rate of gas generation
- Instantaneous mixing of motor exhaust and the volume of gas in the piston
- Negligible thermal loss to the piston tube
- Negligible reduction of motor thrust by the piston internal pressure
- Friction is neglected
- Gas leakage is neglected
- Assume that the air volume between piston tube and support tube is vented

Discussion of methods to represent friction and leakage are included in [3], [8], and [9].

5 ROCKET MOTOR PROPERTIES

This project focused on the Estes C6 motor. This motor was selected due to the size of the measuring altimeter/accelerometer and the carrier vehicle.

5.1 NAR S&T DATA

Rocket motor thrust-vs-time curves and related data were initially obtained from the NAR Standards and Testing data on the NAR web site[6]. This data includes digitized thrust-vs-time points for a typical motor from the batch of motors tested. Other data includes propellant mass and total impulse. The thrust versus time curve for an Estes C6 motor is shown in Figure 5.1-1.

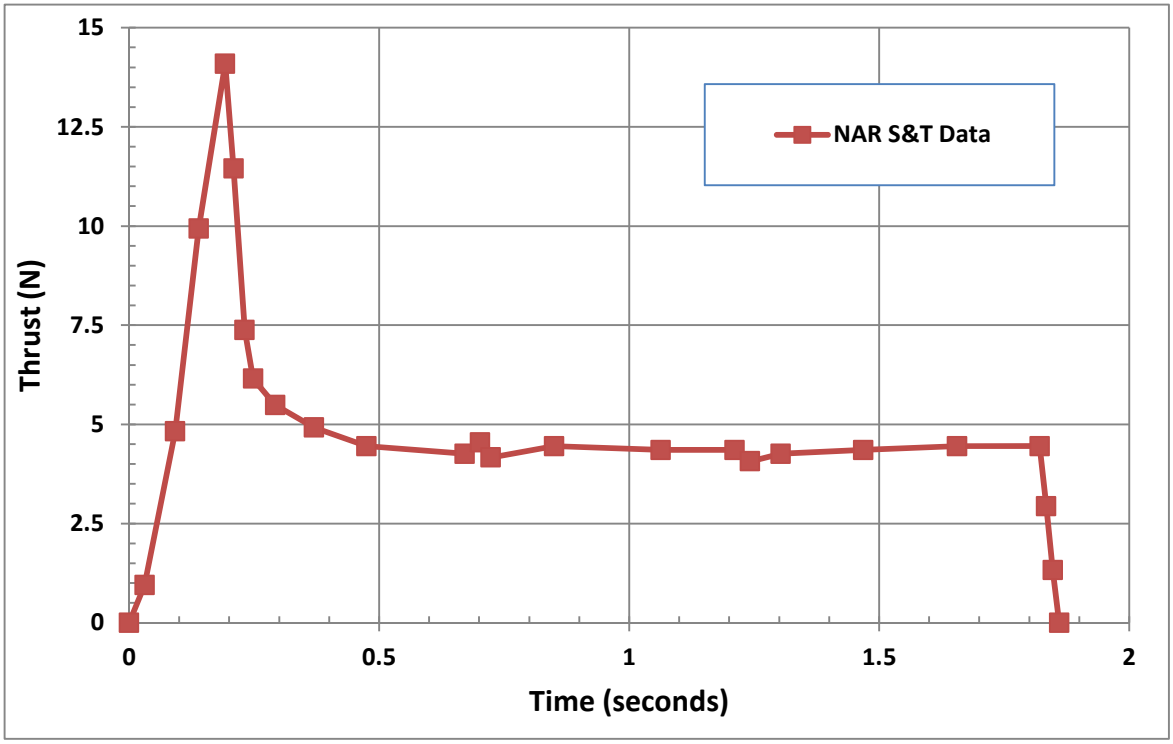

Figure 5.1-1. Thrust versus time for the Estes C6 motor from NAR S&T.

Early results from the piston analysis program indicated that the predicted behavior of the piston was very sensitive to the digitization of the thrust-time curve and total impulse. To provide smoother definition of the thrust and impulse

[6] http://www.nar.org/standards-and-testing-committee/nar-certified-motors/

versus time, the initial portion of the thrust-time curve was fit with a 3rd order polynomial curve. The raw data and curve fit results are shown in Figure 5.1-2.

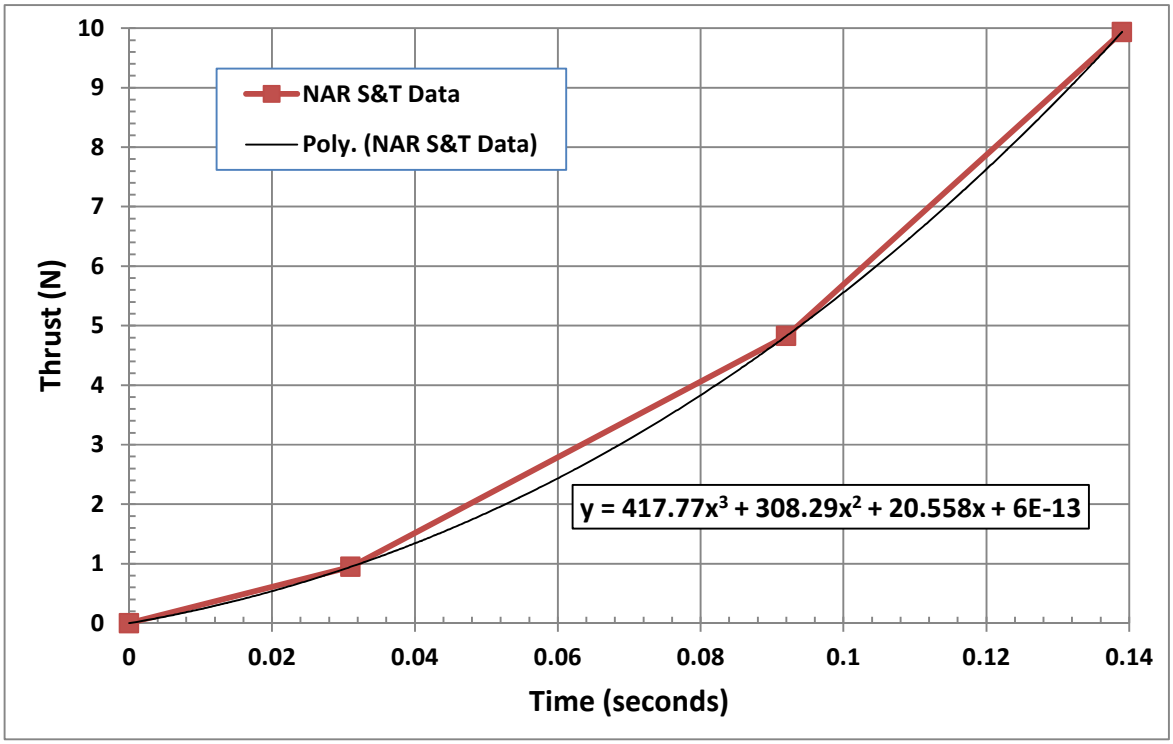

Figure 5.1-2. Curve fit of the initial portion of the Estes C6 thrust-time data.

Using the curve fit data, motor thrust during the initial portion of the thrust-time curve (up to 0.14 seconds) can be calculated as:

$$F_m = 20.558\,t + 308.29\,t^2 + 417.77\,t^3$$

Total impulse during the initial portion of the thrust-time curve can be calculated by integrating the above equation:

$$I_m = 10.279\,t^2 + 102.76\,t^3 + 104.44\,t^4$$

It should be noted that the NAR S&T data is representative for the motors that were tested. The published thrust-vs-time data represents one motor (or an average motor) from the set of tested motors. Some variation is expected between motors within a batch. Larger variations may occur between batches of motor. Finally, commercially produced black powder may vary over the years due to chemicals available. Recently produced motors may have some differences

compared to the motors tested by NAR S&T (in 1995 for the Estes C6 motor). New static test data is described in the following section.

5.2 NEW STATIC TESTING

New static testing of Estes C6 motors was performed for this project. A simple test stand was developed using a Vernier Lab Pro data acquisition system[7] and a Dual-Range Force Sensor (0-10 N or 0-50 N)[8]. Data was acquired at a sampling rate of 1,000 samples/second to provide high resolution of the thrust-time curve.

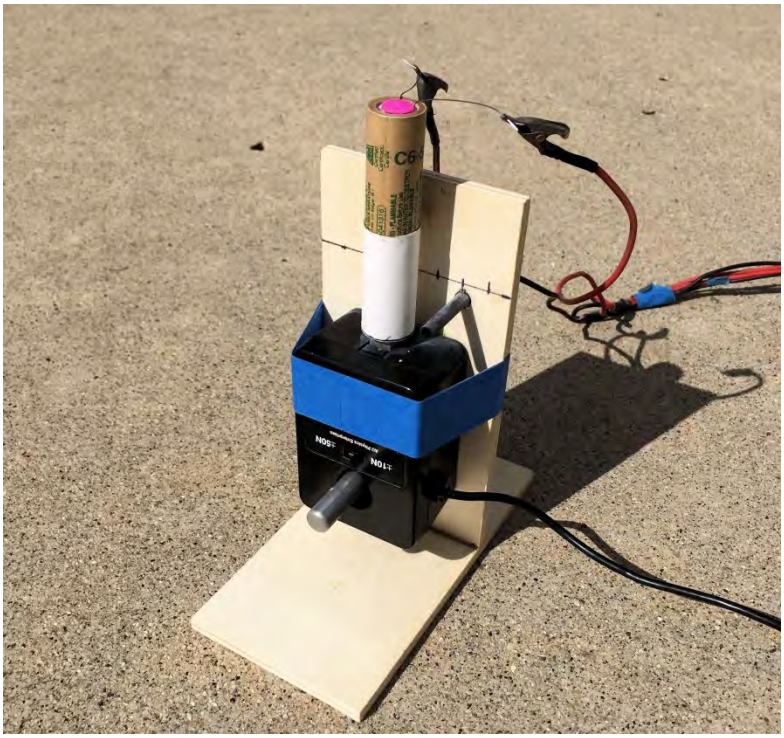

Figure 5.2-1. New static testing was performed for Estes C6 motors.

Three Estes C6-3 motors were tested (motor code A041316). Tests #1 and #2 were performed using the 0-50 N range selected of the force sensor. This allowed the entire thrust-time curve (peak thrust ~14 N) to be measured. Test #3 was performed using the 0-10 N setting of the force sensor to provide higher resolution for low thrust values.

The thrust-time curves from the three static tests (along with NAR S&T data) are shown in Figure 5.2-2 (and Appendix B). The new thrust-time curves were very

[7] http://www.vernier.com/products/interfaces/labpro/
[8] http://www.vernier.com/products/sensors/force-sensors/dfs-bta/

repeatable. Note that the peak thrust data from test #3 was clipped at ~12 N due to using the higher sensitivity (0-10 N) setting of the force sensor.

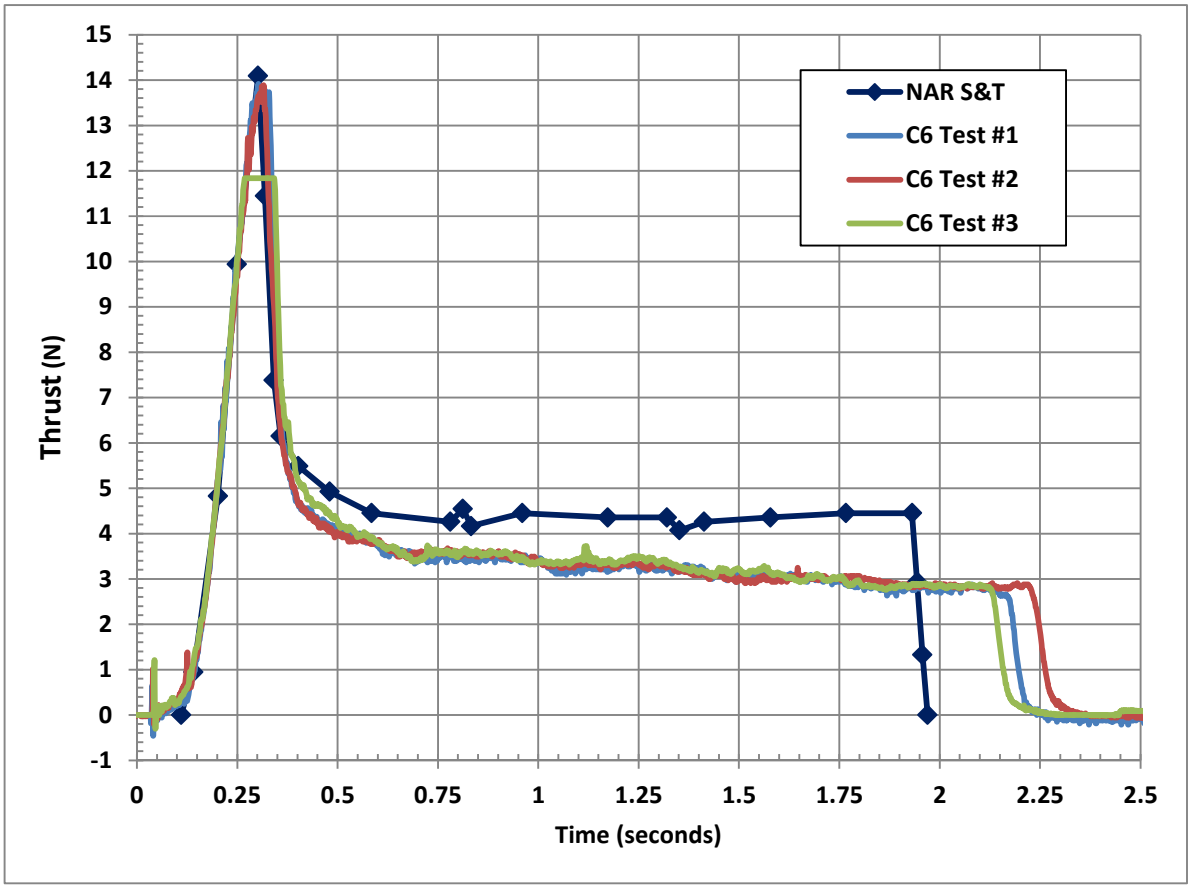

Figure 5.2-2. The thrust-time curves from the three new tests were repeatable.

The initial portions of the thrust-time curves are shown in Figure 5.2-3. The ramp-up information was very repeatable. As shown in Figure 5.2-4, a 5th order polynomial can accurately represent the initial portion of the thrust-time curve (up to 0.20 seconds):

$$F_m = 5.2388\,t - 168.89\,t^2 + 2373.1\,t^3 + 5303.5\,t^4 - 36759\,t^5$$

Total impulse during the initial portion of the thrust-time curve can be calculated by integrating the above equation:

$$I_m = 2.6194\,t^2 - 56.297\,t^3 + 593.28\,t^4 + 1060.7\,t^5 - 6126.5\,t^6$$

These values were used for predicting/analyzing flight responses (see Section 8).

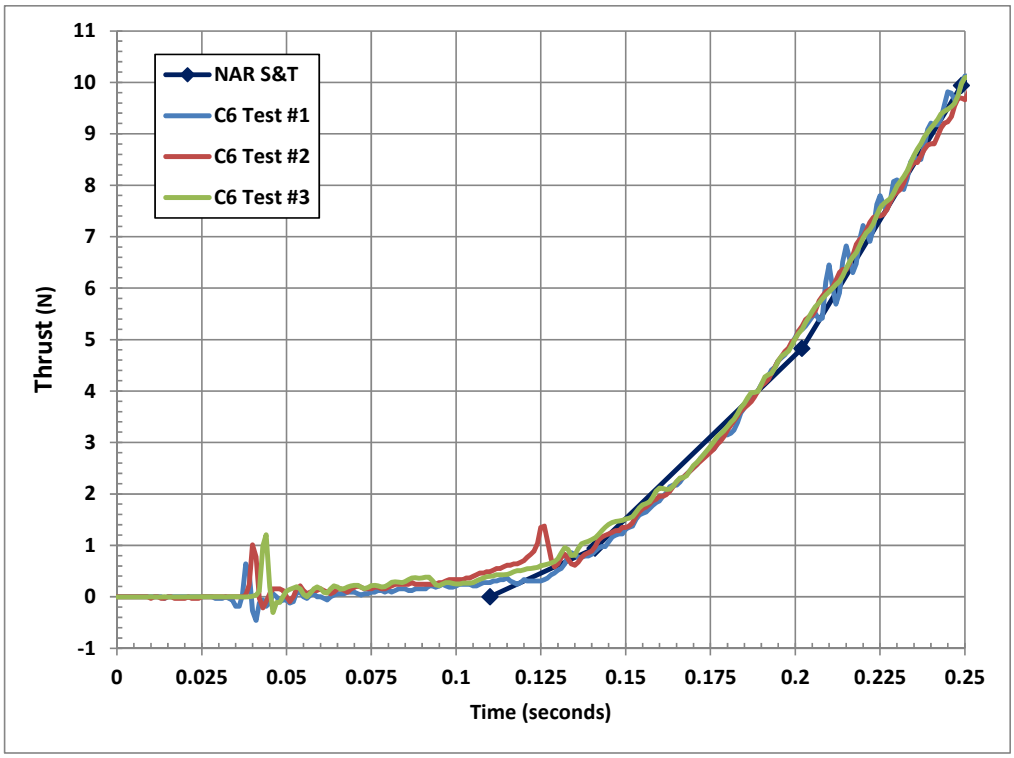

Figure 5.2-3. The initial portion of the Estes C6 thrust-time curves was repeatable.

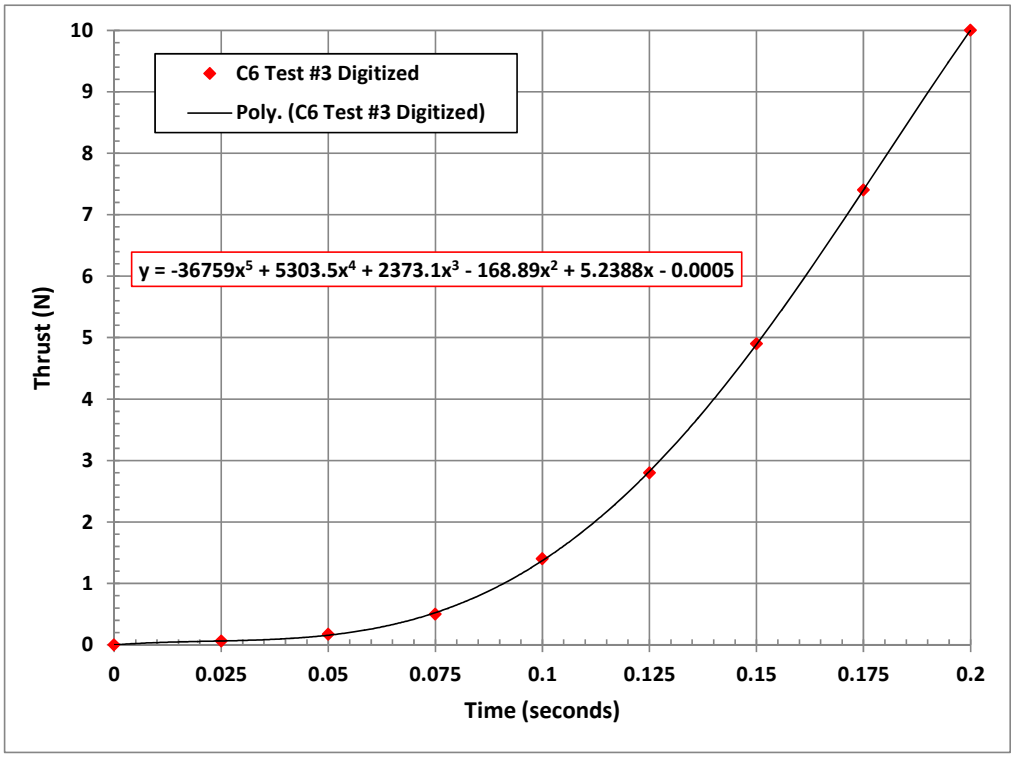

Figure 5.2-4. A 5th order polynomial curve was fit to the initial portion of the C6 thrust-time curve.

6 DEFINITION OF FLIGHT EXPERIMENT

The flight experiment included the following items:

- Flight instrumentation (altimeter/accelerometer)
- Flight test vehicle
- Piston launcher

6.1 FLIGHT INSTRUMENTATION

A Raven altimeter by Featherweight Altimeters [11] was used to measure the flights. This altimeter includes a modern pressure sensor to measure altitudes to ±0.3% accuracy. The altimeter, shown in Figure 6.1-1, is 1.80" long x 0.8" wide x 0.55" thick. The mass of the altimeter, its "Power Perch" mounting system and battery, and a lite ply mounting plate was 25.4 grams.

The Raven altimeter includes 3-axis accelerometers. In the axial (vertical) direction, the accelerometer range is ±70G, and its sampling rate is 400 Hz. As will be shown, the typical piston phase of flight lasts approximately 0.1 seconds. A sampling rate of 400 Hz will provide up approximately 40 data points within the piston phase of flight.

Figure 6.1-1. The Raven 3 altimeter includes an axial accelerometer that measures ±70G at a 400 Hz sampling rate.

6.2 FLIGHT TEST VEHICLE

The design of the flight test vehicle is shown in Figure 6.2-1. The model used a BT-60 body tube to accommodate size of the Raven altimeter. The model included separate bays for the altimeter and an optional payload. The vehicle was built with lite ply fins attached using through-the-wall mounting to be light yet rugged for many flights. The mass of the model (w/o motor, altimeter, or optional payload) was 80.8 grams (2.85 ounces). The mass including the altimeter was 106.2 grams (3.75 ounces).

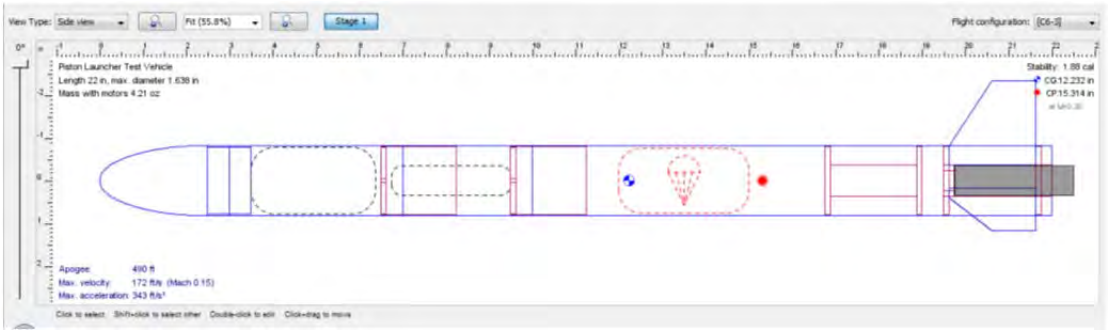

Figure 6.2-1. The flight test vehicle included separate bays for the altimeter and the optional payload.

6.3 PISTON LAUNCHER

The piston support tube was a 36” aluminum tube with a 0.5” outside diameter. The same support tube was used for all flights.

The piston tubes (34” long) were T-20 paper body tubes by Totally Tubular, purchased from www.eRockets.biz. The piston tube had a single paper centering ring (18 mm engine block) at the aft end. Two 1/4” diameter holes were punched in the tube forward of the aft centering ring to allow venting of gas between the support tube and the piston tube.

A floating head was used at the top of the piston tube. The piston head was printed from plastic using an Objet 30 polyjet 3D printer[9]. The outer diameter of the piston head was sized to provide an easy slip fit within the T-20 tube.

A new piston tube and a new piston head was used for each flight. This eliminated potential issues with accumulated gunk/debris.

[9] http://www.stratasys.com/3d-printers/design-series/objet30

The piston component lengths (36” support tube, 2” tall base, 34” piston tube) were such that the aft end of the rocket motor rested on the floating head prior to ignition. This resulted in a very small initial volume.

Piston launches were performed “naked” without support guides around the rocket vehicle. Winds were low on all test flights (< 4 MPH). A typical flight setup is shown in Figure 6.3-1.

Figure 6.3-1. The piston test model was attached to the piston launcher without lateral supports.

On all piston launched flights, the piston tube cleared the piston support rod. The piston tube landed nearby the piston support rod after flight. A typical post-flight arrangement is shown in Figure 6.3-2.

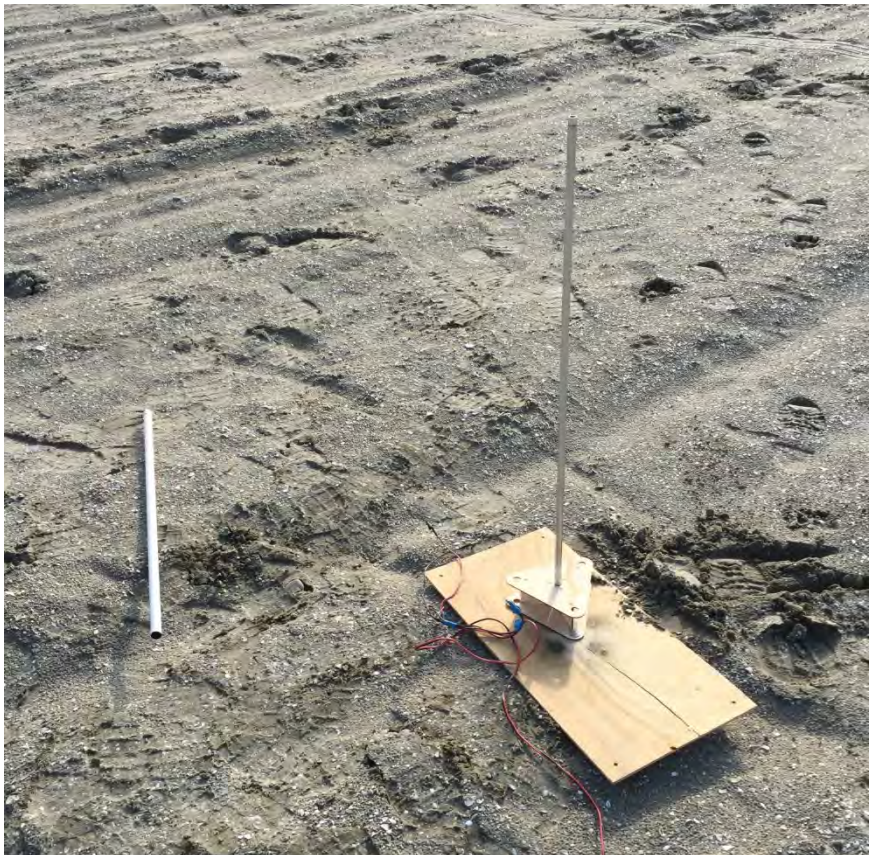

Figure 6.3-2. The piston cleared the piston support rod on all flights.

7 FLIGHT DATA

Three sets of flights were performed:

- Baseline model, without a piston launcher
- Baseline model, 34” T-20 piston launcher
- Model with payload, 34” T-20 piston launcher

The flights are described in the following sections.

7.1 WITHOUT PISTON LAUNCHER

Two flights were made without a piston launcher. The baseline vehicle (no additional payload) was used. C6-3 motors were used (motor code A061915).

Axial accelerations from the two flights are compared to the predicted (OpenRocket, using NAR S&T motor data) axial acceleration in Figure 7.1-1. The flight data has generally good agreement to analysis predictions. The flight “steady state” acceleration was slightly lower than predicted, and the motor burn time was somewhat longer than the NAR S&T data. This is consistent with the results from the new static testing of current C6-3 motors.

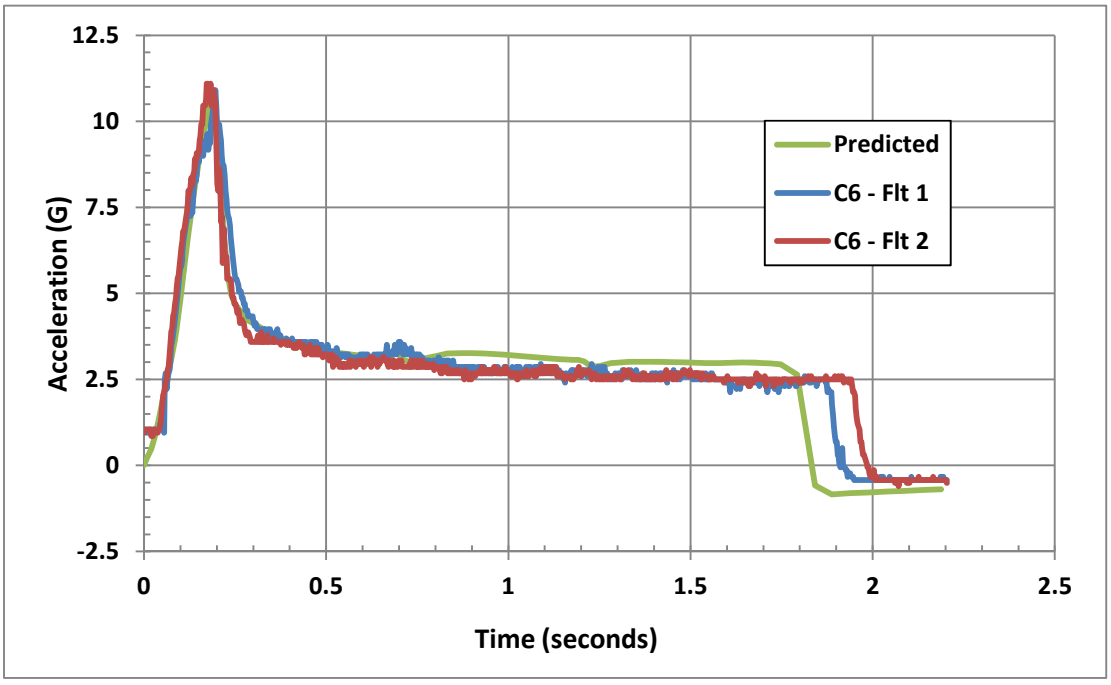

Figure 7.1-1. The axial acceleration from the flights without piston agreed well with the predictions from OpenRocket.

7.2 PISTON LAUNCHED

Three flights were made using the baseline vehicle (no additional payload) and a piston launcher. C6-3 motors were used (motor code A061915).

Axial accelerations from the three flights are shown in Figures 7.2-1 through 7.2-3. The accelerations during the piston phase of flight were significantly higher than without a piston. Peak acceleration during the piston phase of flight exceeded 30 G's.

All three flights showed a noticeable "blip" (as high as 15 G's) before the main ramp-up of acceleration. This may have been caused by the igniter heat/gas or by gas dynamics of a piston launcher with very small initial volume.

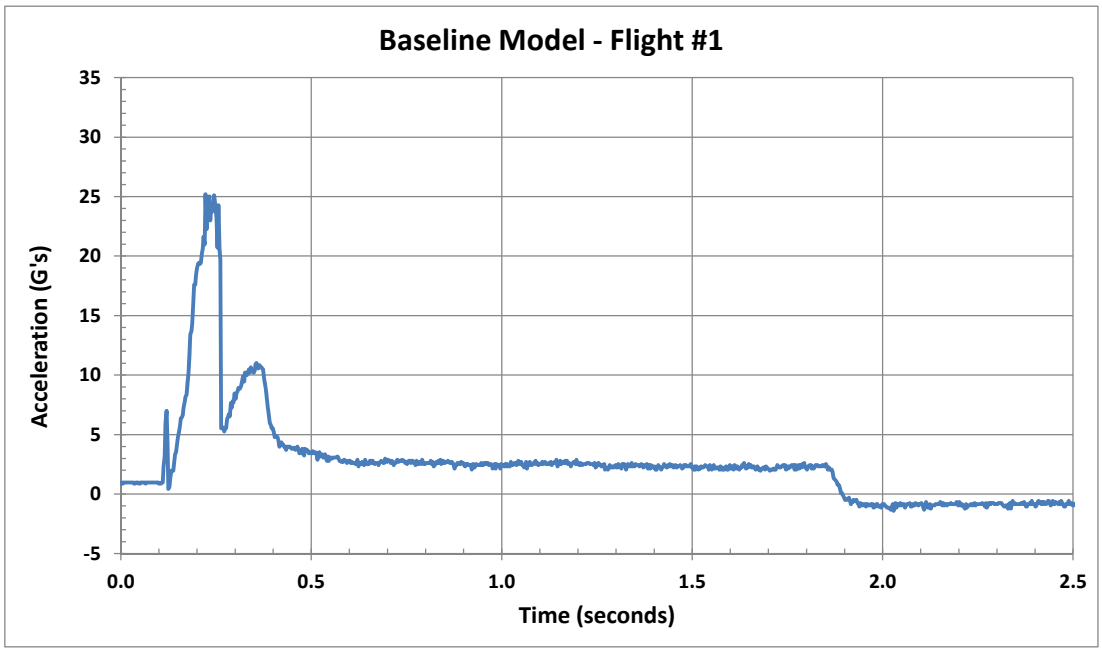

Figure 7.2-1. Baseline model with piston - Flight #1.

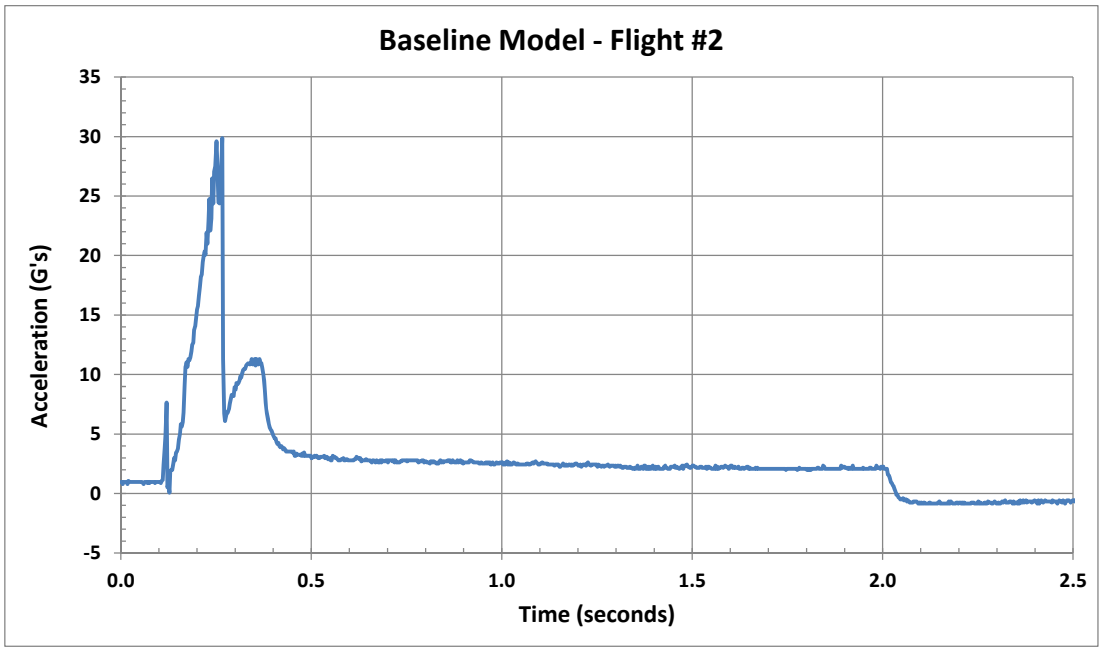

Figure 7.2-2. Baseline model with piston - Flight #2.

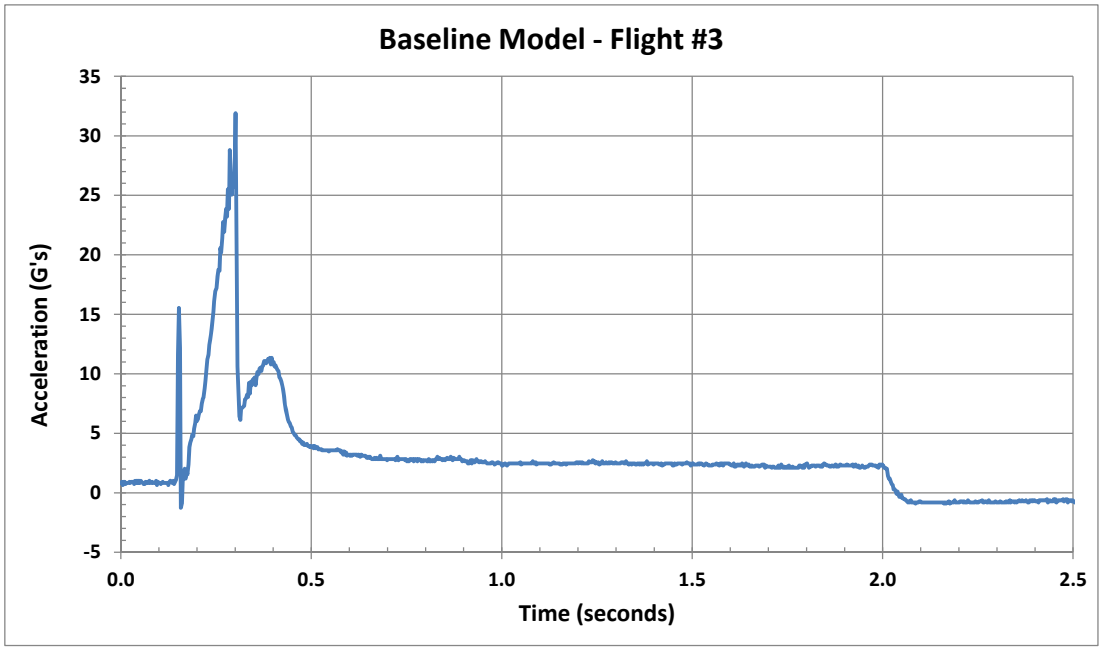

Figure 7.2-3. Baseline model with piston - Flight #3.

The axial accelerations from the three flights are overlaid in Figure 7.2-4. The results from the three flights were repeatable. This may have been helped by using a new piston tube and piston head for each flight (no accumulated buildup of residue or gunk).

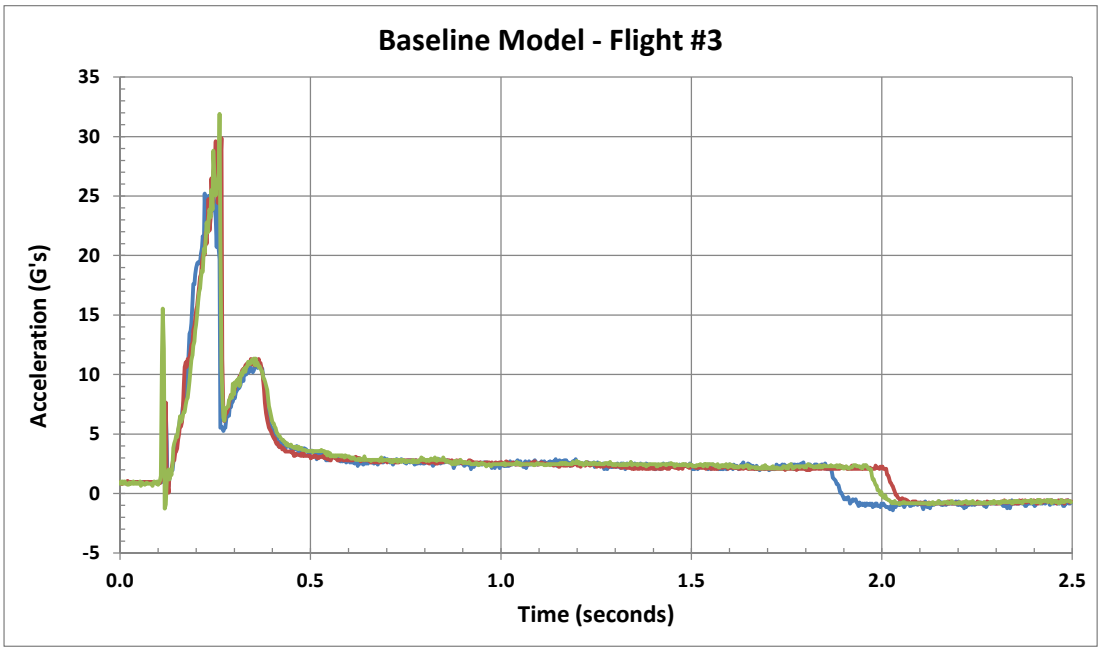

Figure 7.2-4. Baseline model with piston - Flights #1-3 overlaid.

Figure 7.2-5 shows the piston phase of flight. As noted earlier, the piston performance was repeatable. Somewhat surprisingly, there was no significant acceleration "blip" when the piston tube (with floating head) was ejected from the model following separation from the piston support rod.

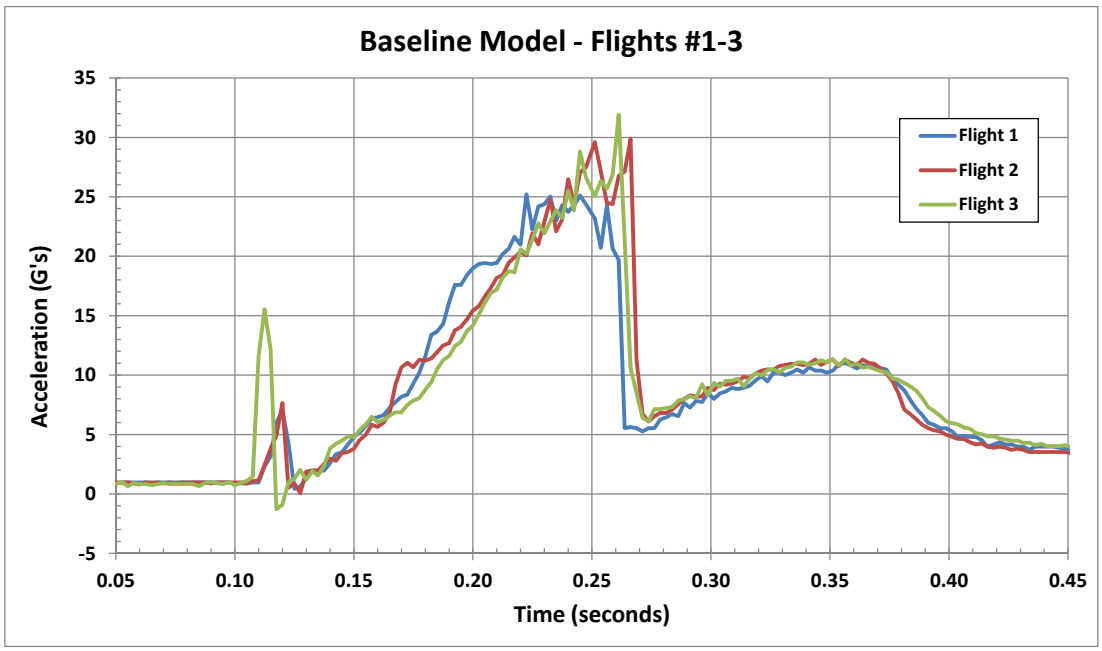

Figure 7.2-5. Baseline model with piston – overlay of Flights #1-3.

Velocities were calculated by numerically integrating the accelerations. As shown in Figure 7.2-6, the velocity at the end of the piston operation was ~19-20 m/sec.

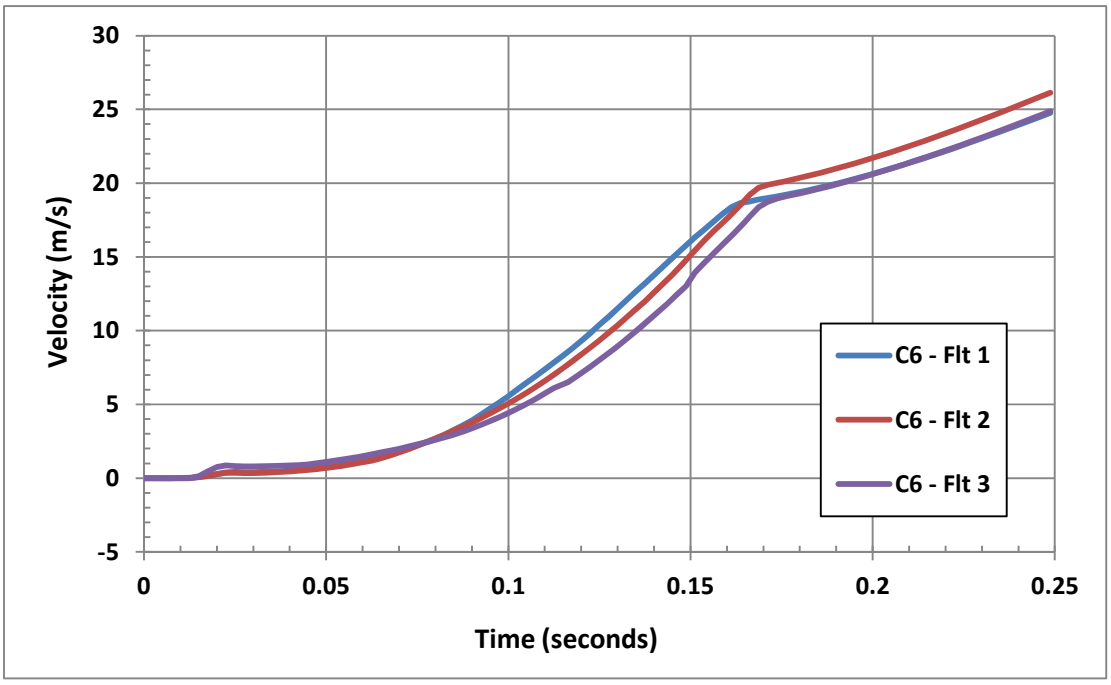

Figure 7.2.6. The velocity at the end of the piston tube travel was 19-20 m/sec.

7.3 PISTON LAUNCHED, WITH PAYLOAD

A NAR-standard payload (28 grams) and mounting materials (33.0 grams total) were placed into the payload bay of the model. Two flights were made using the vehicle (with payload) and a piston launcher. C6-3 motors were used (motor code A061915).

Axial accelerations from the two flights are shown in Figures 7.3-1 and 7.3-2. Peak acceleration during the piston phase of flight exceeded 25 G's. This was only slightly lower than the accelerations for the baseline model (without payload).

The axial accelerations from the two flights are overlaid in Figure 7.3-3. The results were repeatable. A detailed view of the piston phase of flight is shown in Figure 7.3-4.

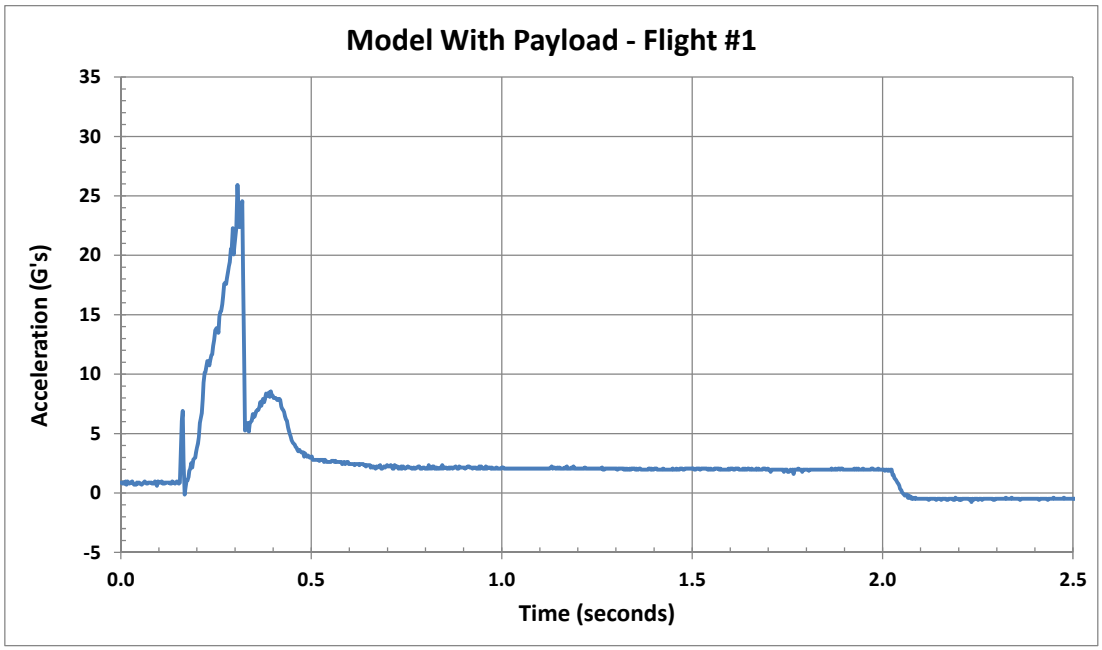

Figure 7.3-1. Model with 1 ounce payload - Flight #1.

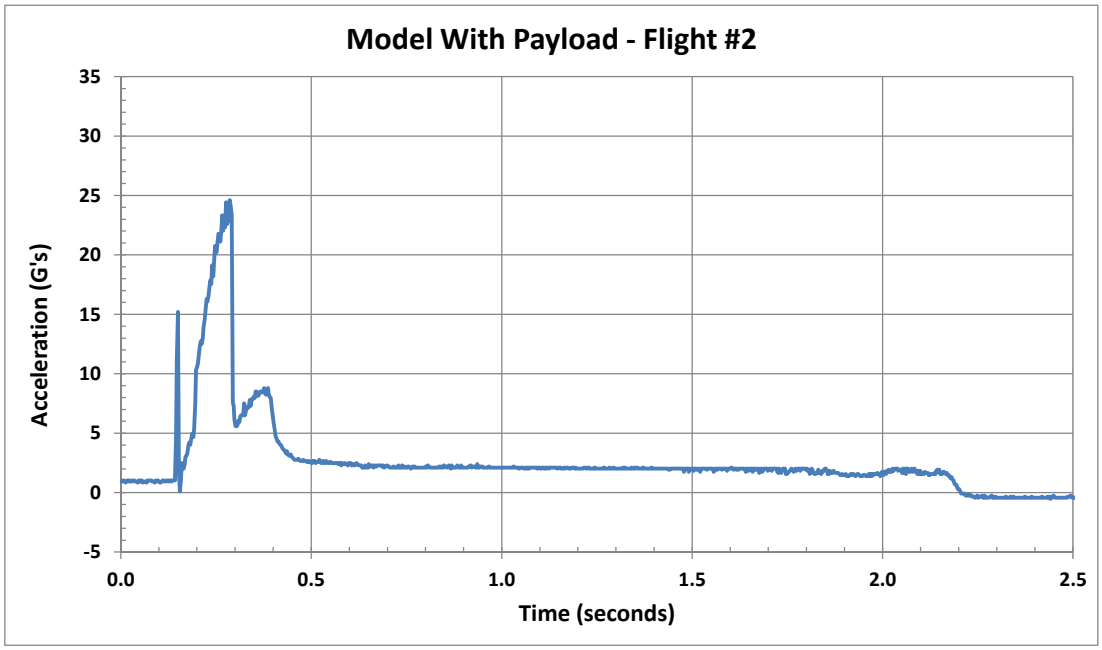

Figure 7.3-2. Model with 1 ounce payload - Flight #2.

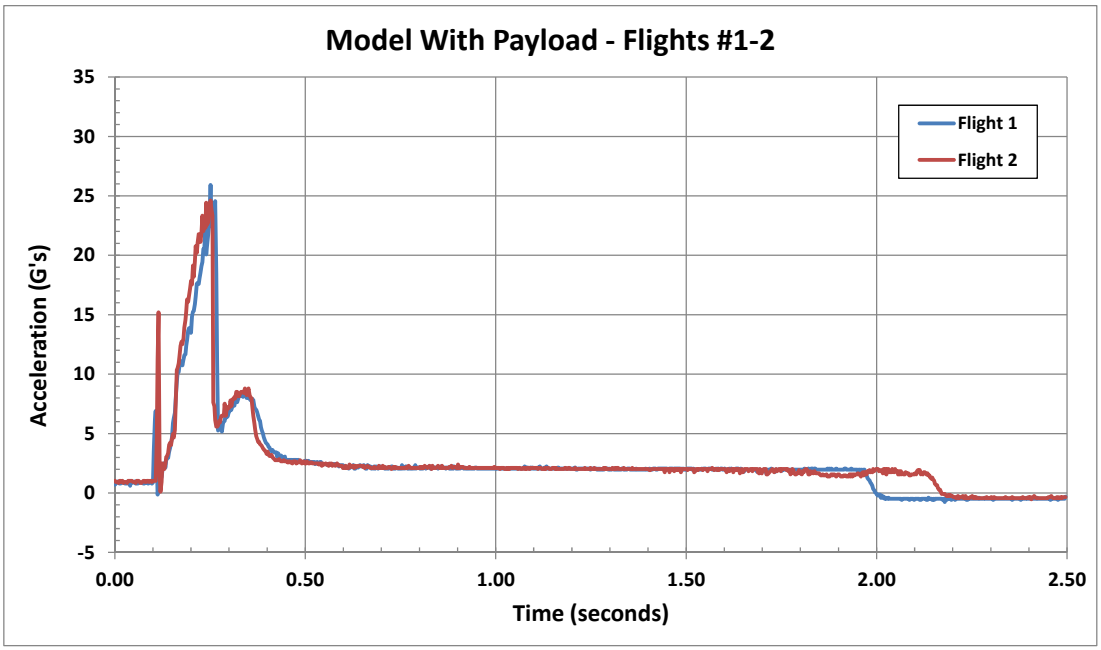

Figure 7.3-3. Model with 1 ounce payload – overlay of flights #1-2.

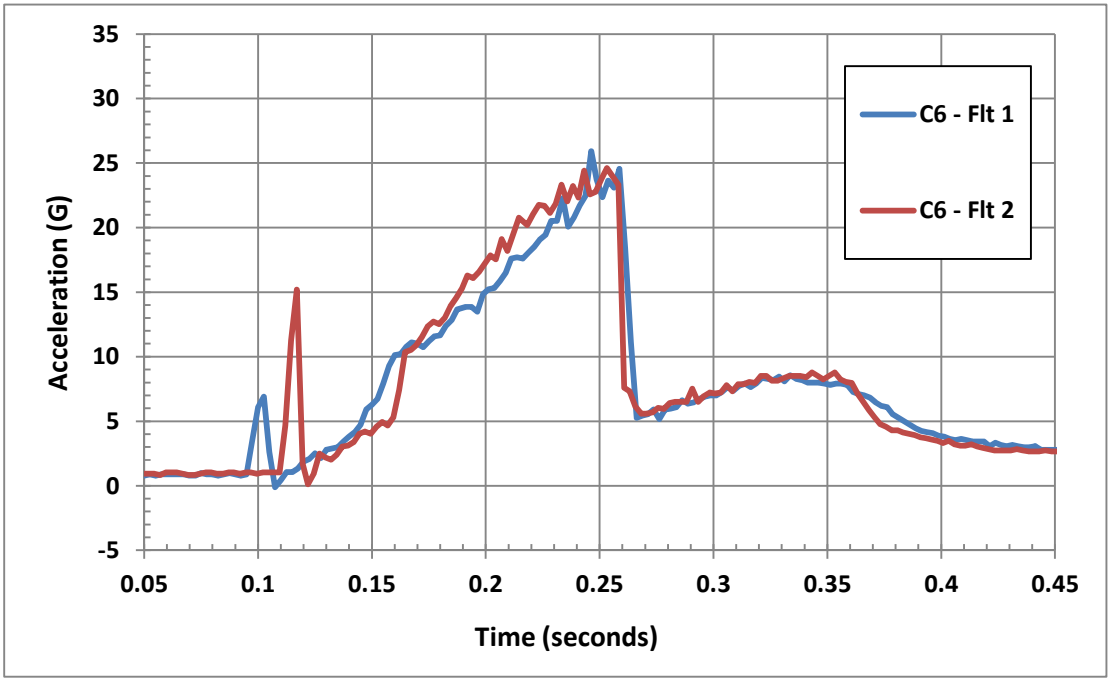

Figure 7.3-4. Model with 1 ounce payload – overlay of flights #1-2.

Velocities were calculated by numerically integrating the accelerations. As shown in Figure 7.3-5, the velocity at the end of the piston operation was ~18 m/sec.

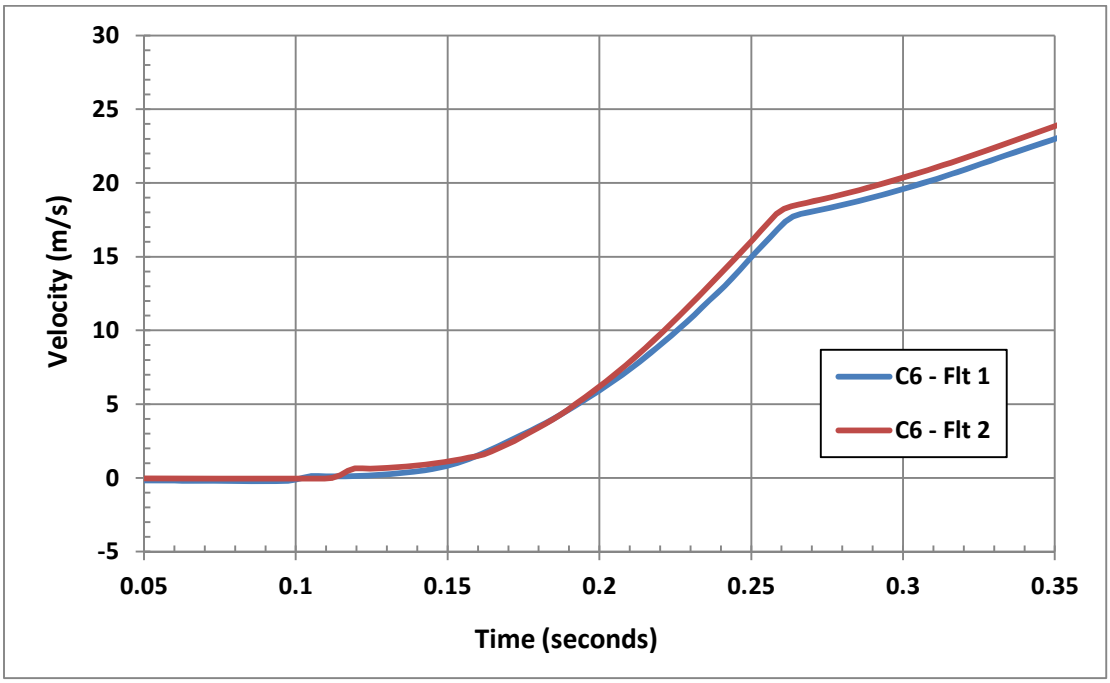

Figure 7.3.5. The velocity at the end of the piston tube travel was ~18 m/sec.

7.4 POST-FLIGHT INSPECTION

One of the piston tubes was cut open and inspected. As shown in Figure 7.4-1, there was "gunk" near the top of the tube. Beyond ~7-8", there was very little debris. The outside surface of the top ~4" of the tube showed minor blistering of the white outer layer of the tube. This indicated that the tube got hot but not so hot as to significantly char or burn the paper tube. Surprisingly, there was a small amount of black (soot) buildup at aft vent holes. This was presumably caused by some exhaust gas leaking past the piston head and being forced out the vent holes as the piston traveled upwards.

One of the 3D-printed piston heads is shown in its post-flight condition in Figure 7.4-2. There was some gunk on the top of the cap, but there wasn't any charring or melting of the plastic cap. The cap would likely be reusable after some cleaning.

Figure 7.4-1. Only the top ~8” of the piston tube had noticeable launch effects.

Figure 7.4-2. The piston floating head cap did not show any significant charring or melting.

8 CORRELATION OF ANALYSIS AND FLIGHT DATA

8.1 ANALYSIS METHODOLOGY

The piston launcher performance was calculated using an updated version of the "Piston Launcher Performance Program" (PLPP) developed by Geoff Landis [3]. The program was implemented as an Excel spreadsheet to allow for rapid changes of model variables and to provide immediate graphs of results. As noted in Section 4.3, effects of friction and heat loss were assumed to be negligible and were not included. The numerical algorithm for solving the differential equations of motion was upgraded to use Huen's method[10] (also known as the Improved Euler method). The integration time step was set to a small value (0.0001 seconds) to provide a numerically stable solution.

8.2 BASELINE MODEL – INITIAL CORRELATION

The first correlation analysis used a table lookup function to calculate the motor thrust and total impulse as a function of time. The table lookup function performed a piecewise linear interpolation using the data points in the NAR S&T thrust-time curve (shown previously in Figure 5.2-1). This is the typical process used in most altitude simulation programs.

The initial correlation of the piston launch acceleration was not very good. As shown in Figure 8.2-1, the predicted acceleration was much higher than the flight data. The analysis results also had very large spikes that did not occur in the flight data. It was observed that the abrupt changes in the predicted acceleration coincided with the data points in the NAR S&T thrust-time curve. This implied that a piecewise linear lookup function was too coarse to accurately represent the motor behavior during the piston phase of flight.

The next step in the correlation process used a polynomial curve to calculate the motor thrust and total impulse as a function of time. A polynomial curve provided a smooth, continuous thrust-time (and impulse-time) definition and avoided the abrupt changes of a piecewise linear method.

[10] https://en.wikipedia.org/wiki/Heun%27s_method

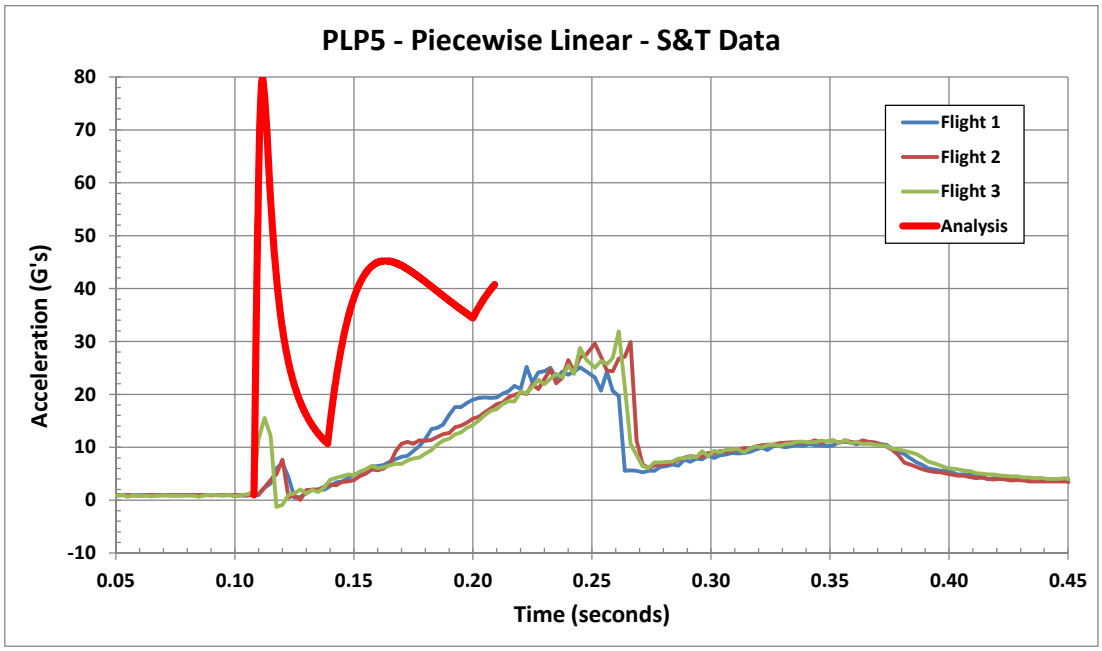

Figure 8.2-1. Using a piecewise linear lookup of thrust and impulse provided analysis results that did not match flight data.

As shown in Figure 8.2-2, results using the polynomial curve approach were better but still did not provide a satisfactory match to flight data. The initial peak to 23 G's was higher than flight. After the initial peak, the slope of the acceleration curve was similar to flight, but, the total piston time was much shorter than flight.

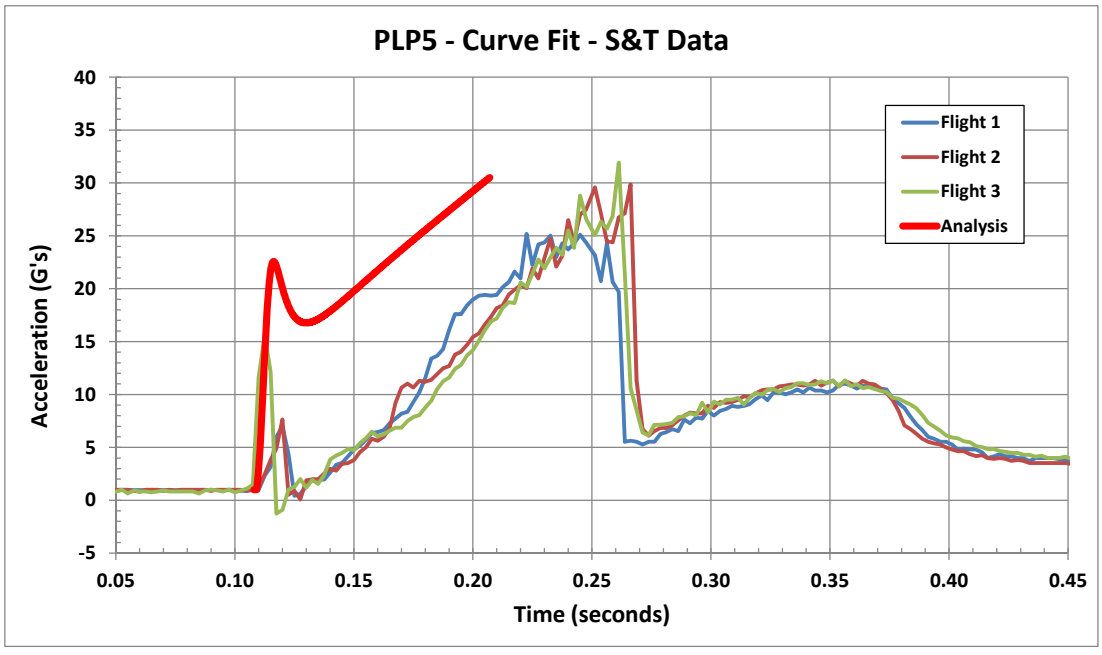

Figure 8.2-2. Using a polynomial curve fit of motor thrust and impulse eliminated the abrupt changes caused by using a piecewise linear lookup.

The results in Figure 8.2-2 implied that a more refined definition of the motor's low thrust characteristics was needed. For most applications, the low level thrust behavior isn't of much interest. However, piston launchers capture the motor exhaust gas immediately after ignition. Therefore, the low level thrust behavior is very important for piston launcher performance.

The next correlation step used a curve fit to the motor data from the first static test performed by the author (labeled "C6 Test #1" in Figure 5.2-3). As shown in Figure 8.2-3, the agreement between analysis and flight improved. The peak acceleration improved, and the piston launcher action time (from ignition to piston release) was close. However, the analysis results showed a large dip after the initial peak, and this did not occur in the flight data. This implied that even more refined data was needed to represent the initial performance of the motor.

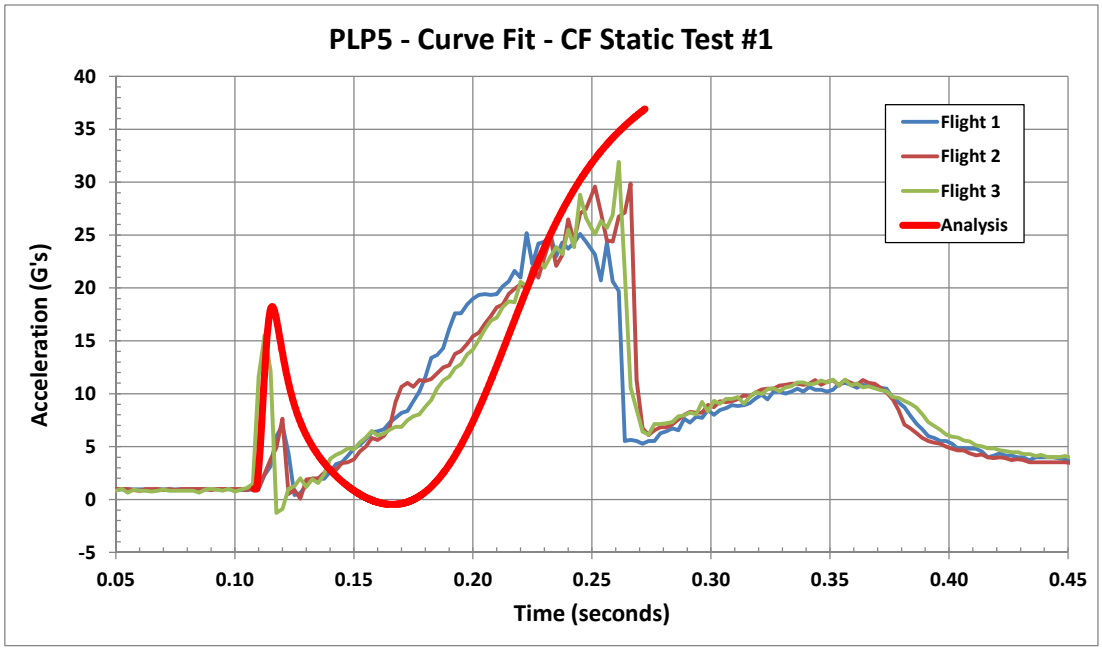

Figure 8.2-3. Curve fit 1st static test

8.3 BASELINE MODEL – FINAL CORRELATION

As described in the previous section, analysis showed that the predicted results were very sensitive to the motor characteristics (thrust and total impulse versus time) following ignition. To provide best results, the motor data from the high resolution static testing (described previously in Section 5.2 and Figure 5.2-4) was used in the analysis.

The analysis predictions of accelerations of the baseline model (without payload) are shown in Figure 8.3-1. The analysis accelerations agreed very well with the flight data.

The analysis predictions of velocities of the baseline model (without payload) are shown in Figure 8.3-2. The analysis velocities agreed very well with velocities calculated from the flight accelerations.

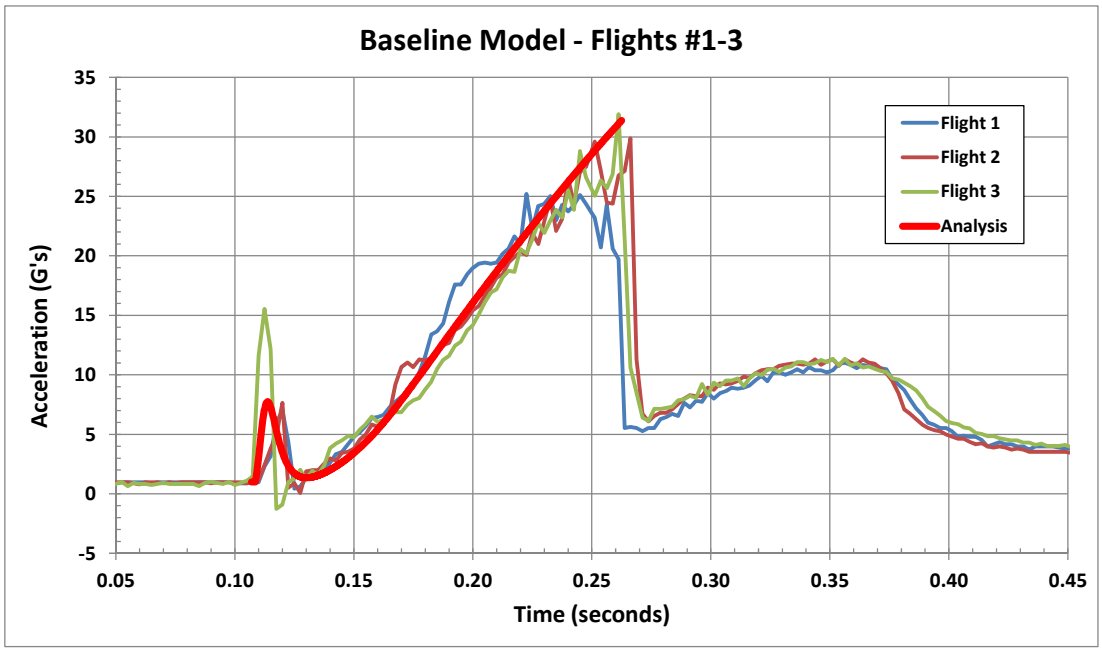

Figure 8.3-1. The predicted accelerations for the baseline model (without payload) agree very well with flight results.

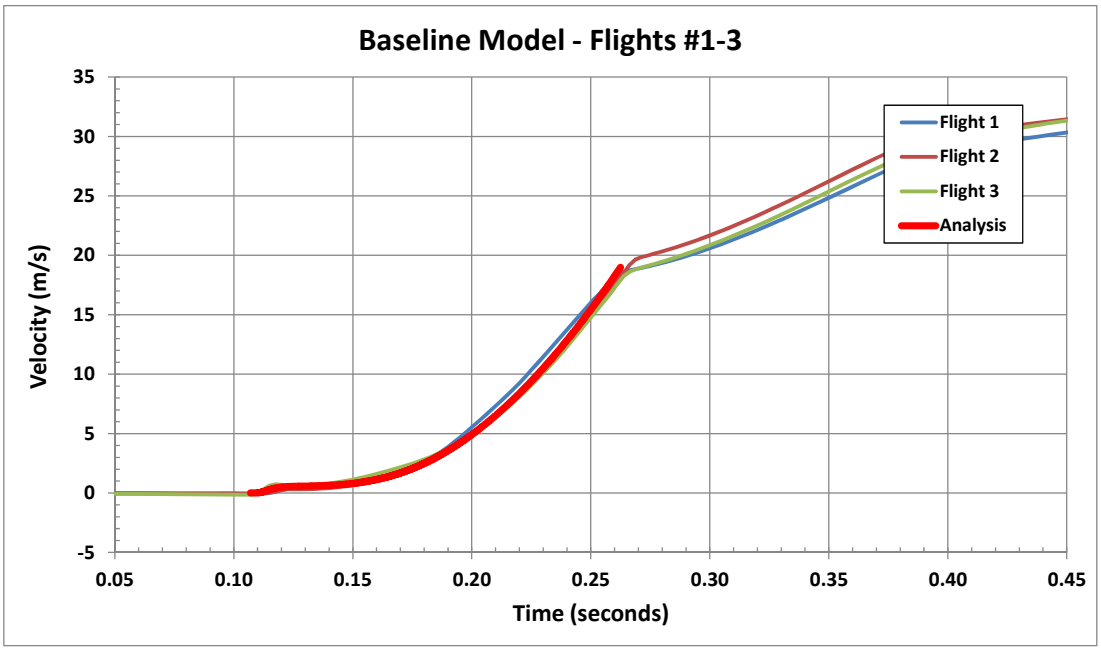

Figure 8.3-2. The predicted velocities for the baseline model (without payload) agree very well with flight results.

8.4 MODEL WITH PAYLOAD

The analysis predictions of accelerations of the model with payload are shown in Figure 8.4-1. The analysis results agree well with the flight data. The analysis results may be somewhat higher than the flight data, particularly towards the end of the piston travel. This might indicate that friction forces or gas leakage were more significant for the heavier model. The analysis predictions of velocities of the model with payload are shown in Figure 8.4-2. The analysis velocities agree well with flight velocities.

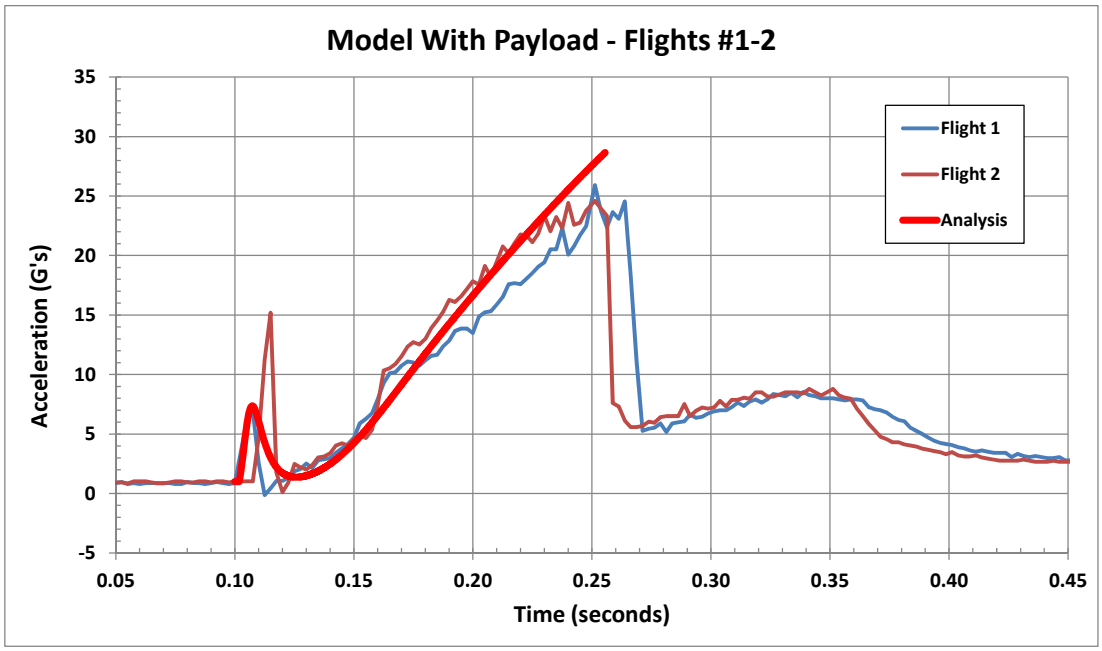

Figure 8.4-1. The predicted accelerations for the model with payload agree well with flight results.

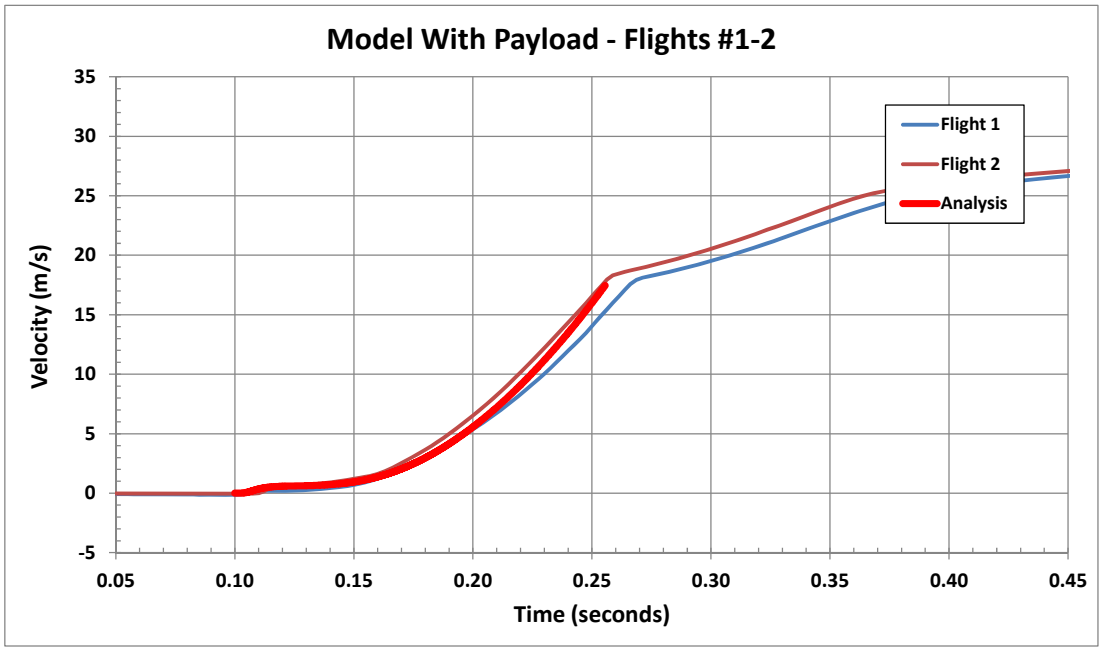

Figure 8.4-2. The predicted velocities for the model with payload agree very well with flight results.

8.5 AUGMENTED THRUST-TIME CURVE

The piston pressure applies an additional force to the rocket. The total force (pressure force plus motor thrust) versus time curves for the baseline model and model with payload are shown in Figure 8.5-1. Note that the total force varied with the mass of the rocket.

The piston pressure force added a significant amount of total impulse:

- Nominal thrust-time curve (motor only): 8.01 N-sec
- Baseline model: 11.20 N-sec (40% increase)
- Model with payload: 11.75 N-sec (46.6% increase)

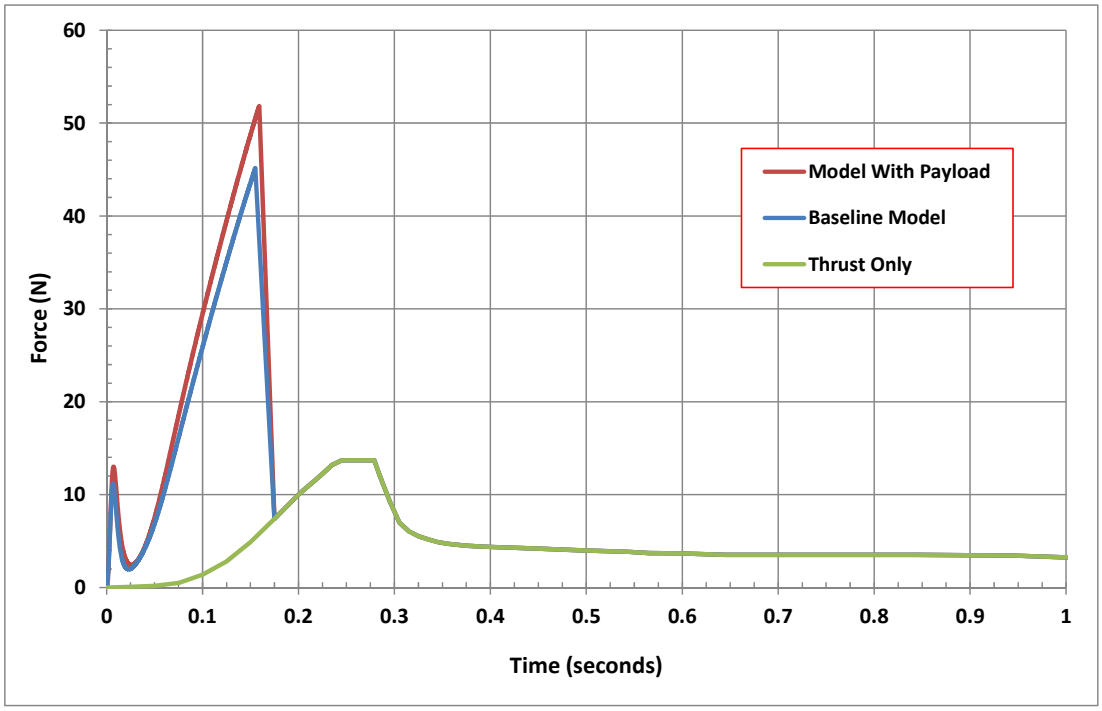

Figure 8.5-1. The piston launcher adds a significant amount of total impulse.

9 SUMMARY AND RECOMMENDATIONS

The objectives of this project were to measure accelerations during piston phase of flight and to compare flight results to analysis predictions. The project successfully achieved both objectives. The project focused on the Estes C6 motor and an 18 mm diameter piston. An altimeter/accelerometer was used to measure axial accelerations during flight. Analysis results were calculated using an updated version of the Piston Launcher Performance Program originally developed by Geoff Landis. New static testing was performed to provide high resolution data for the Estes C6 motor.

Flight data and analysis results were compared. Both accelerations and velocities agreed well when using high resolution thrust-time data. This indicated that the piston program theory was accurate for this class of piston launcher, motor, and model.

There are many related topics that could be that could be explored in future studies:

- Additional motors (13 mm motors, 24 mm motors)
- Additional piston tube diameters (13 mm, 24 mm) and length
- Additional model sizes (lighter, heavier)
- Effect of piston initial volume

10 EQUIPMENT, FACILITIES, AND BUDGET

10.1 EQUIPMENT

The following equipment was used in this project:

- Craft tools (X-Acto knife, razor saws, epoxy, etc.) for construction of the test flight model
- Raven altimeter to record acceleration and altitude

10.2 FACILITIES

An Objet 30 3D printer was used to print the piston heads. Access to the printer was provided by Quartus Engineering Incorporated (www.quartus.com).

10.3 PROJECT BUDGET

The budget for this project is listed in Table 10.3-1. Note that the data acquisition system (Lab Pro unit and force sensor) were purchased by the author for a prior R&D project. No additional funds were spent on these items for the current project.

Table 10.3-1. Budget for this project.

Description	Vendor	Unit	Quan	Total
INSTRUMENTATION				
Raven3 altimeter	Featherweight	$155.00	1	$155.00
Power Perch mounting system	Featherweight	$35.00	1	$35.00
			Subtotal	*$190.00*
STATIC TESTING				
Lab Pro data acquisition unit	Vernier / eBay	$69.99	1	$69.99
Dual range force sensor	Vernier / eBay	$62.00	1	$62.00
C6-3 motors (pack of three)	Estes	$11.79	1	$11.79
			Subtotal	*$143.78*
FLIGHT TESTING				
Carrier rocket (body tube, nose cone)	BMS, Estes	$10.00	1	$10.00
C6-3 motors (pack of three)	Estes	$11.79	3	$35.37
T-20 body tubes	eRockets.biz	$2.50	5	$12.50
CR520-P rings (T-20 engine blocks)	BMS	$0.15	5	$0.75
Piston floating heads (3D printed)	self	$1.28	5	$6.40
			Subtotal	*$65.02*
			Total	**$398.80**

REFERENCES

1. The Barber Team (T-151), “An Investigation of the Dynamics of the Closed-Breech Launcher”, NARAM-14 R&D report, 1972.
2. R.Thoelen, T.Bauer, & P.Porzio, “Optimization of Zero-Volume Piston Launcher”, MITCON, 1973.
3. Landis, Geoffrey, “Investigation of the Physics of the Zero Volume Piston Launcher”, NARAM-17 R&D report, 1975.
4. Charles Weiss & Jeff Vincent, “Floating Head Piston Launcher”, NARAM-28 R&D report, 1986.
5. Charles Weiss & Jeff Vincent, “Optimum Length for a Floating Head Piston Launcher”, NARAM-30 R&D report, 1988.
6. Robert & Peter Always, “Piston Pressure and Massive Models”, NARAM-47 R&D report, 2005.
7. Patrick Peterson/Neutron Fusion Team, “Piston Effect on Thrust Curves”, NARAM-55 R&D report, 2013.
8. Johnsgard, Scott K., Jr, "A Theoretical Analysis of the Operation of Zero Volume and Floating Head Piston Launchers", NARAM-42 R&D report, 2000.
9. Ryan, Jeffrey, “Summary of a Mathematical Model of Zero Volume and Floating Head Piston Launchers”, NARAM-58 R&D report, 2016.
10. Barber, Trip, “Internal Ballistics of Estes C6 Motor”, NARAM-13 R&D report, 1971.
11. Adamson, Adrian, “Raven Users Guide: Updated for the Raven3 Altimeter,” Featherweight Altimeters LLC. http://www.featherweightaltimeters.com/uploads/Raven_Users_Manual_2014May20.pdf

Appendix A

Flight Data

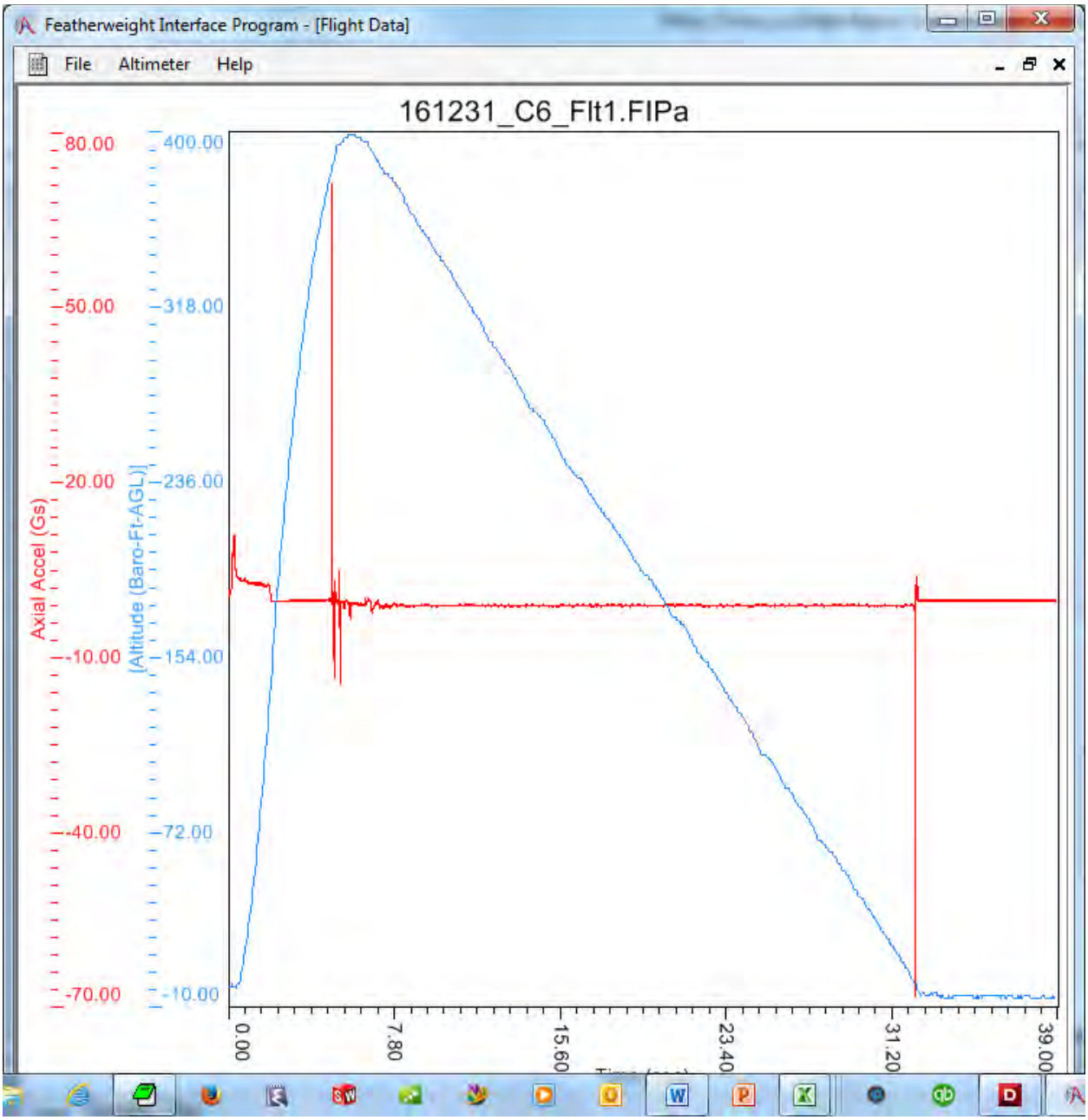

Baseline model, without payload, not piston launched - #1

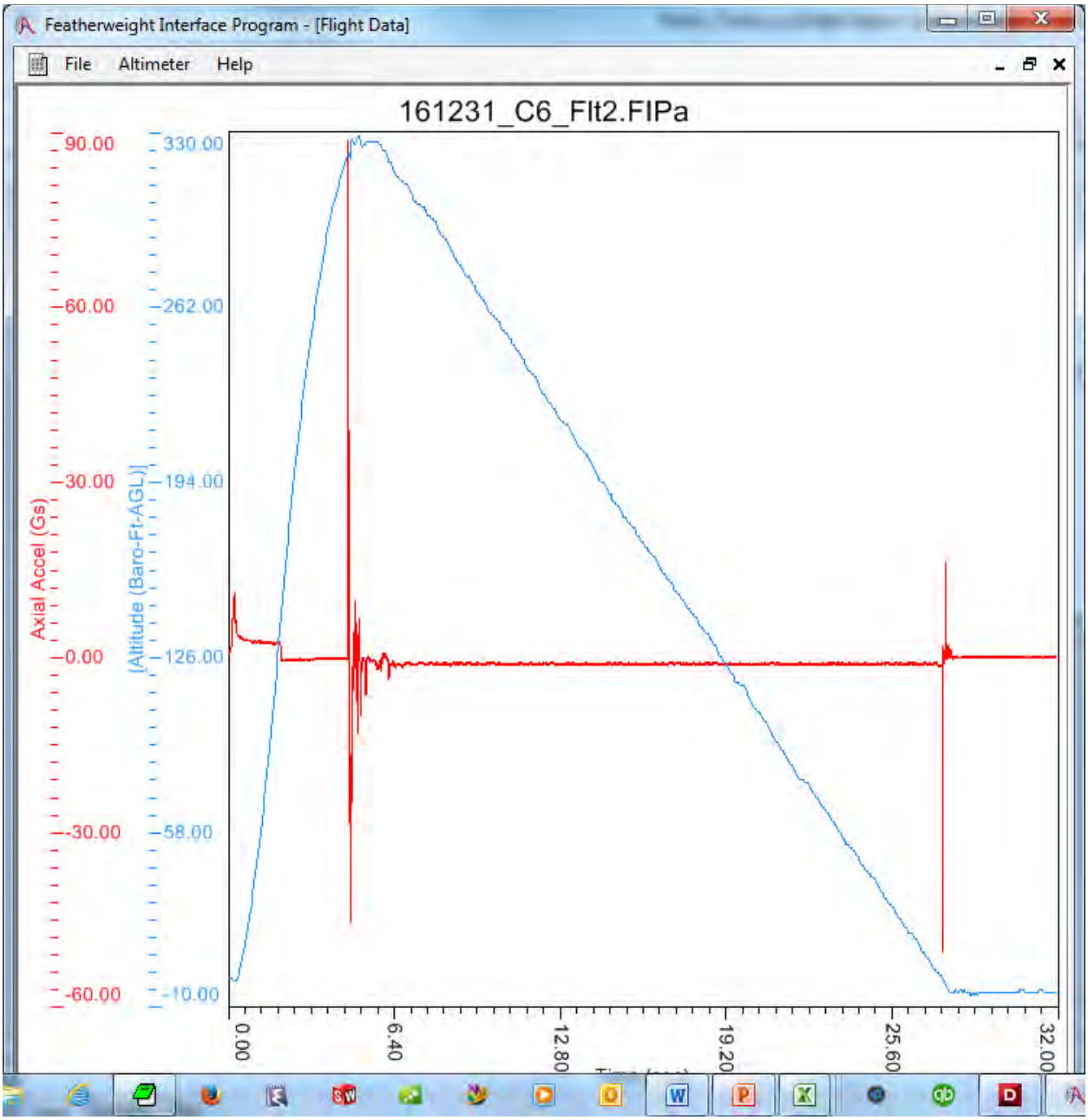

Baseline model, without payload, not piston launched - #2

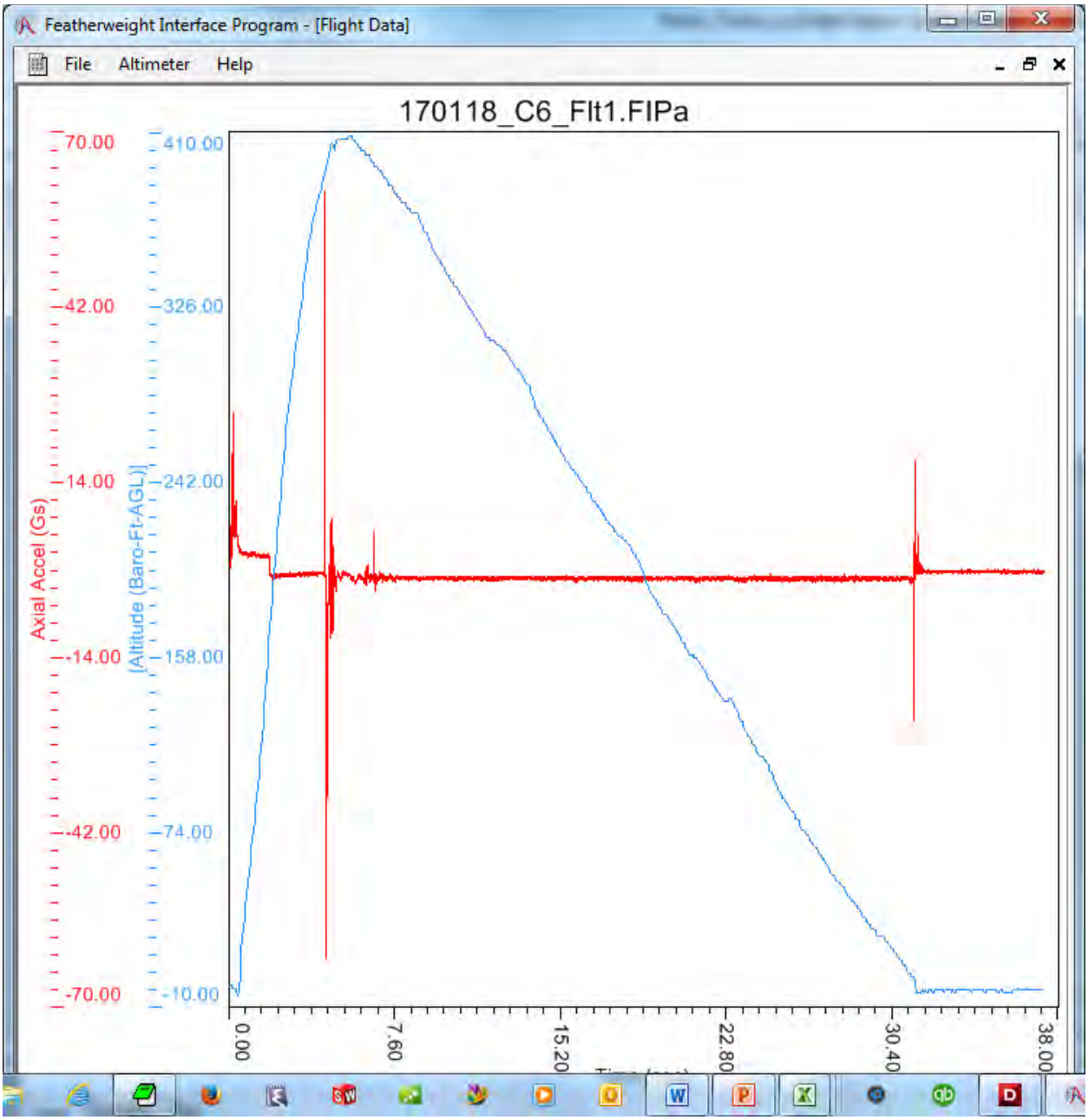

Baseline model (without payload), piston launched - #1

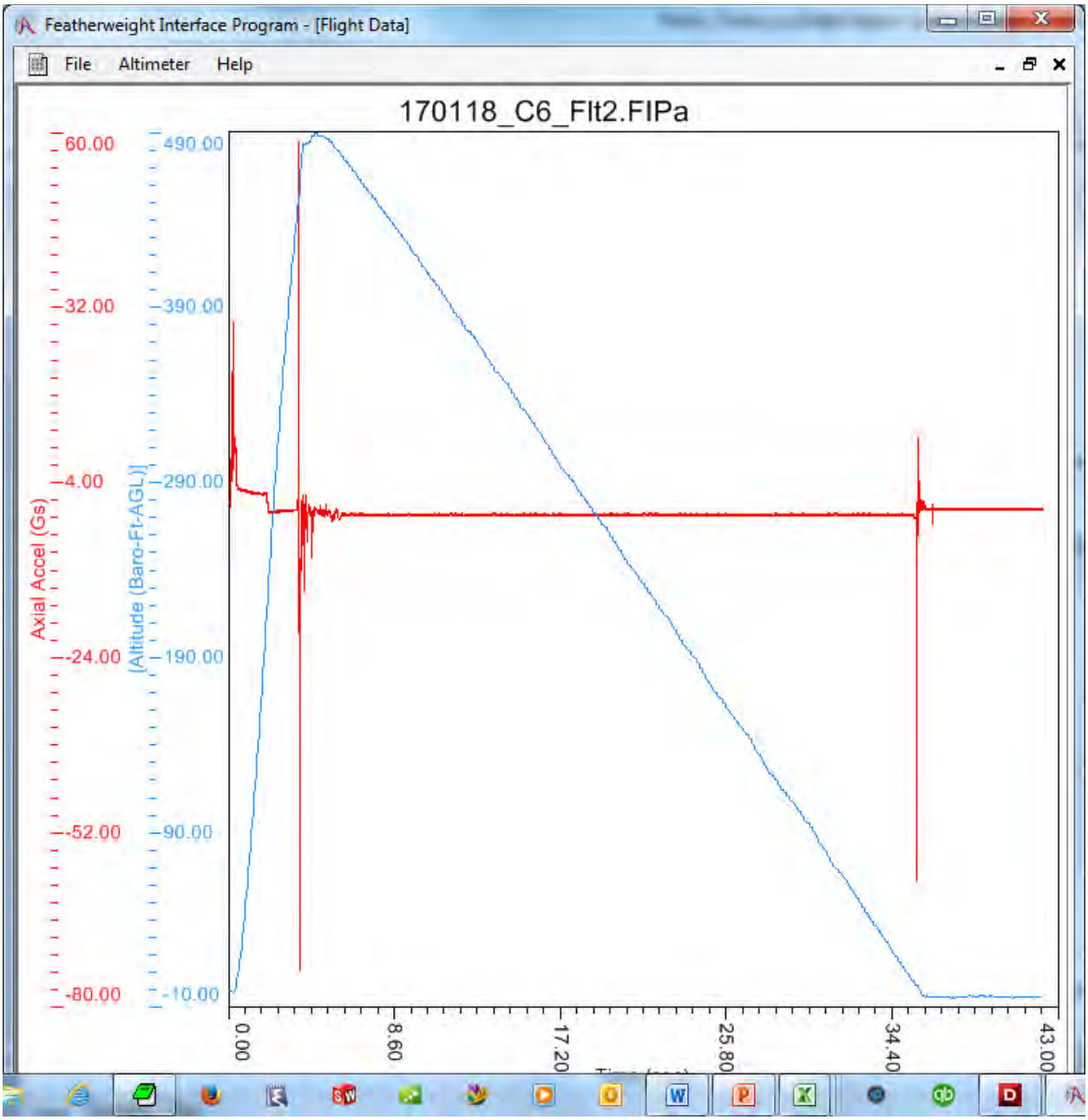

Baseline model (without payload), piston launched - #2

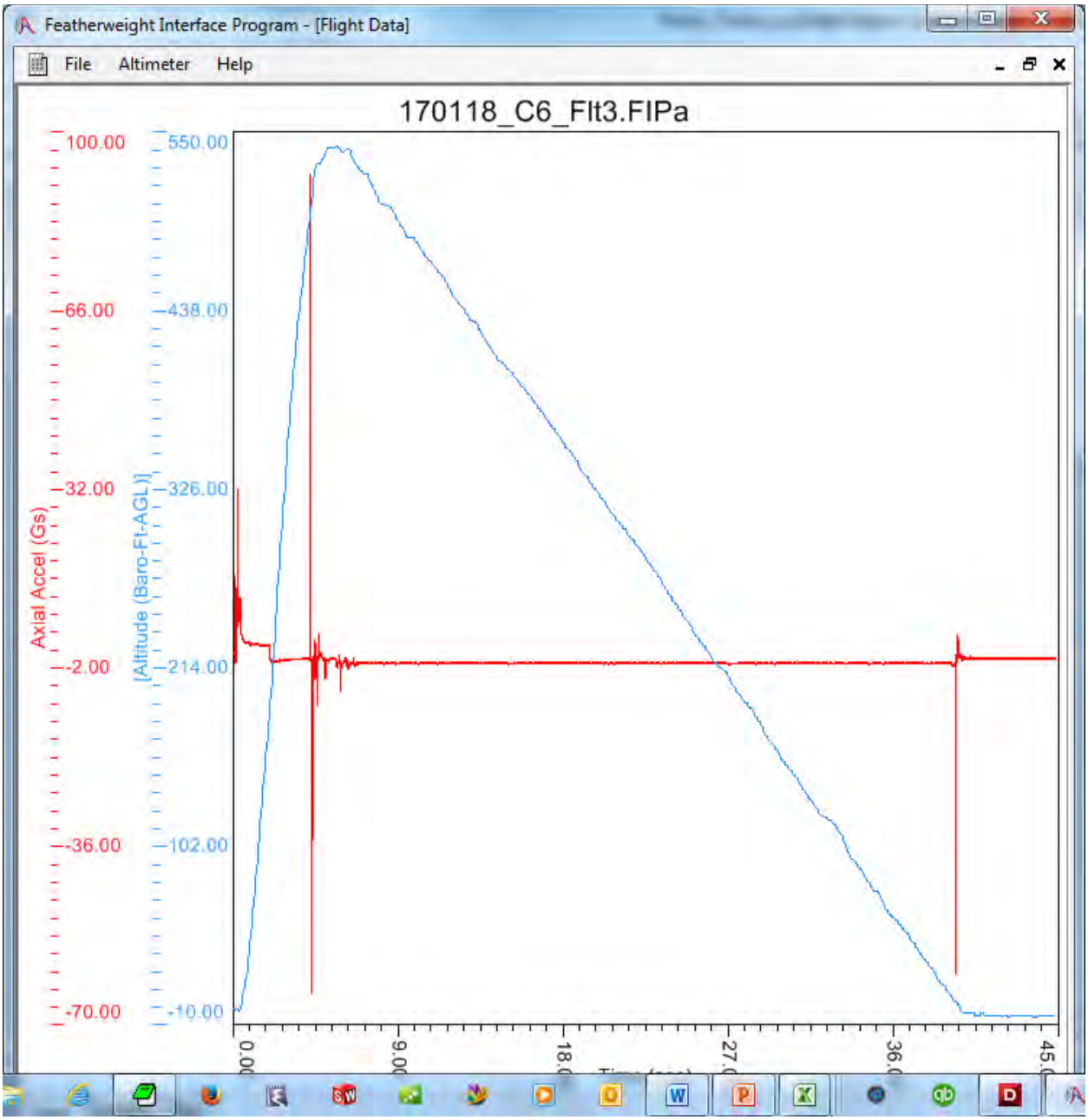

Baseline model (without payload), piston launched - #3

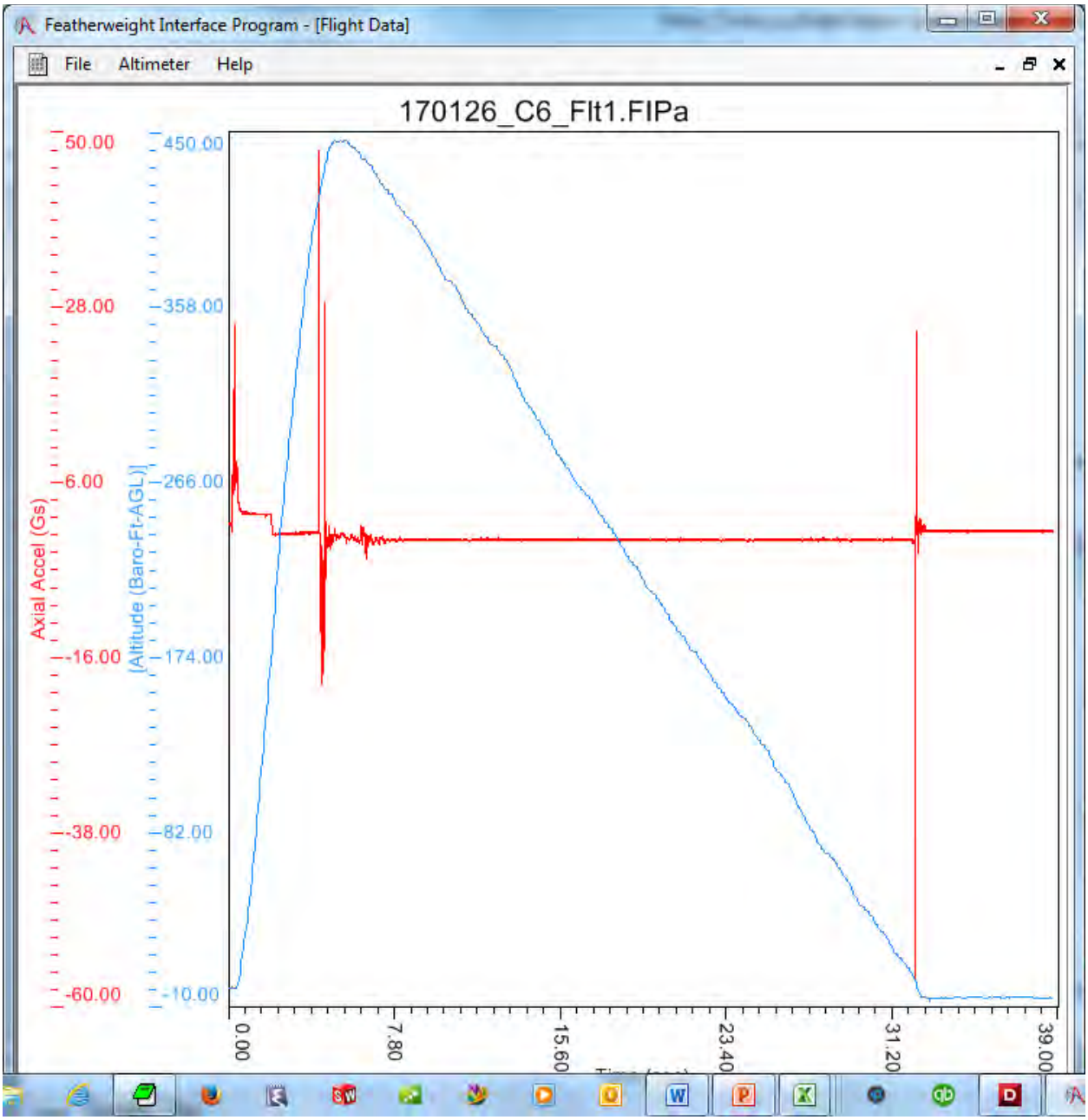

Model with payload, piston launched - #1

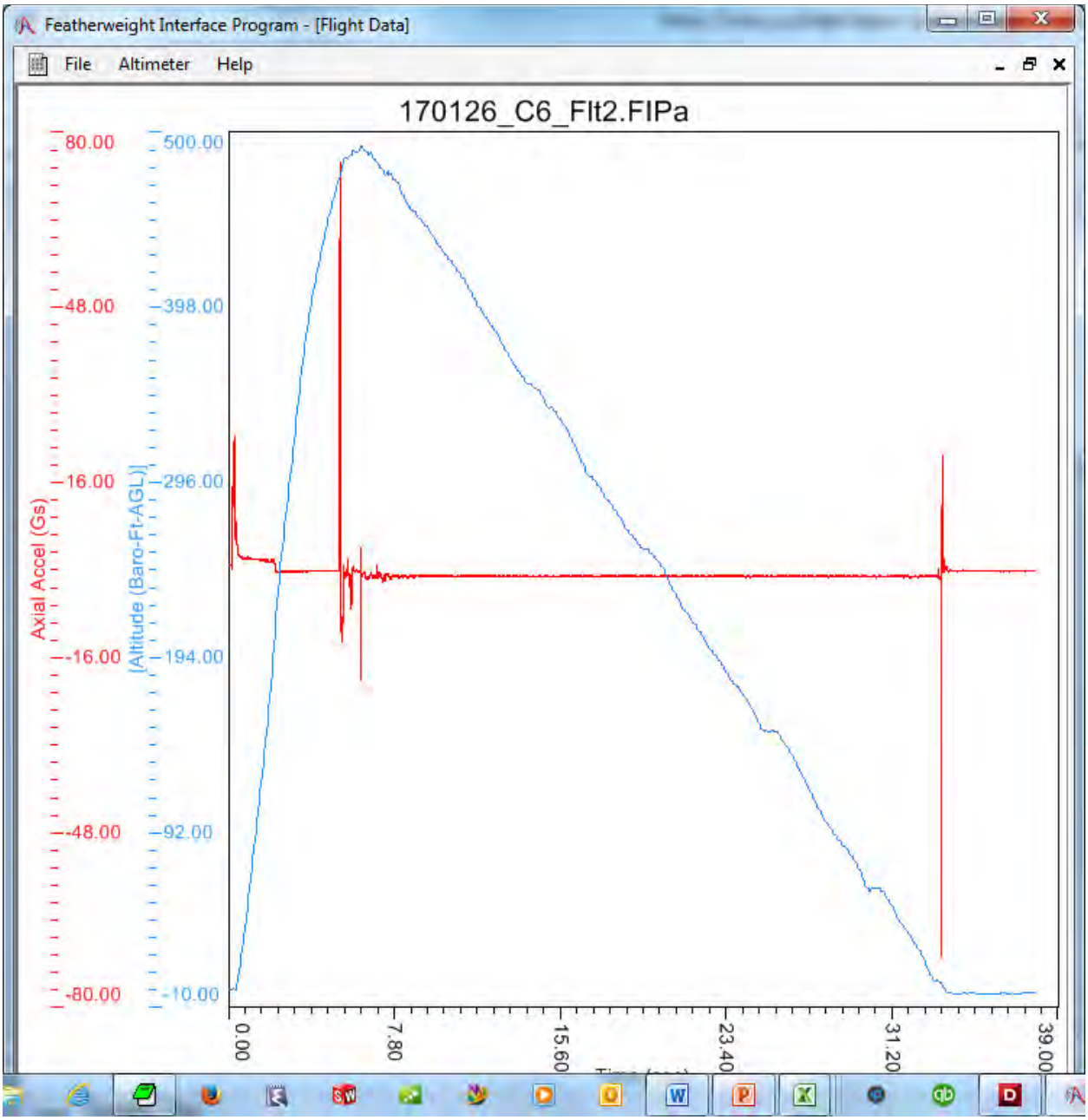

Model with payload, piston launched - #2

Appendix B

Static Test Data

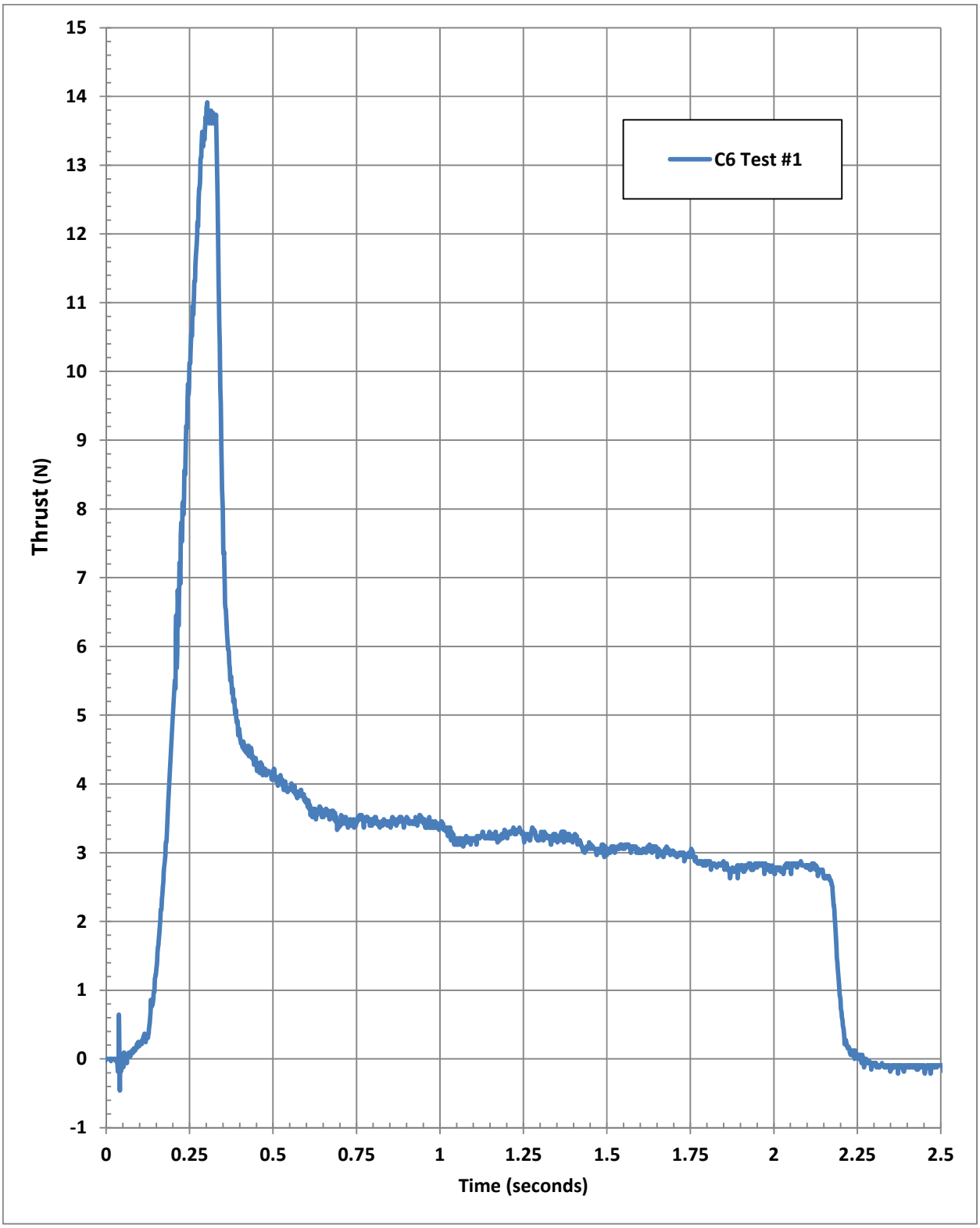

Figure B-1. "C6 Static Test #1".

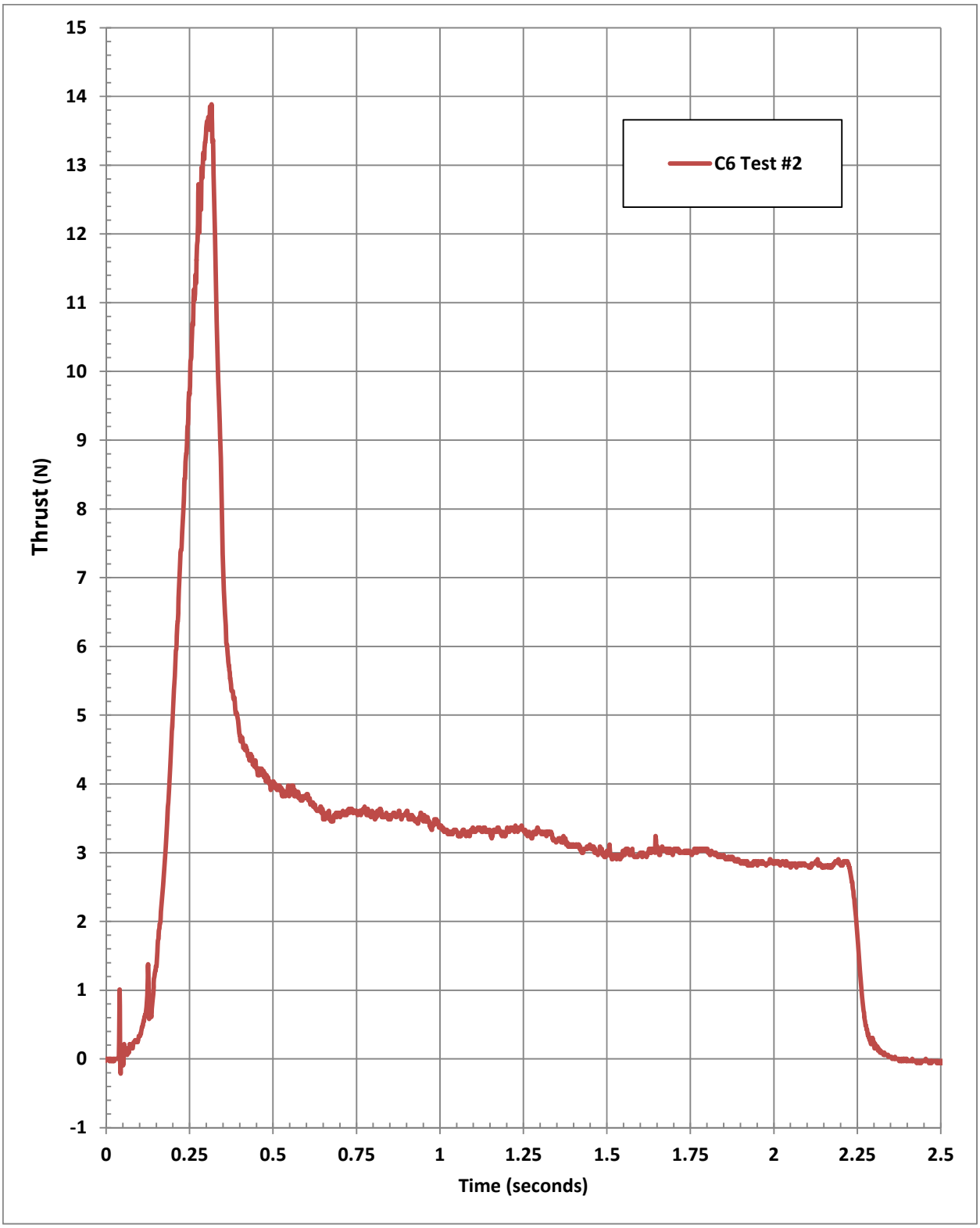

Figure B-2. “C6 Static Test #2”.

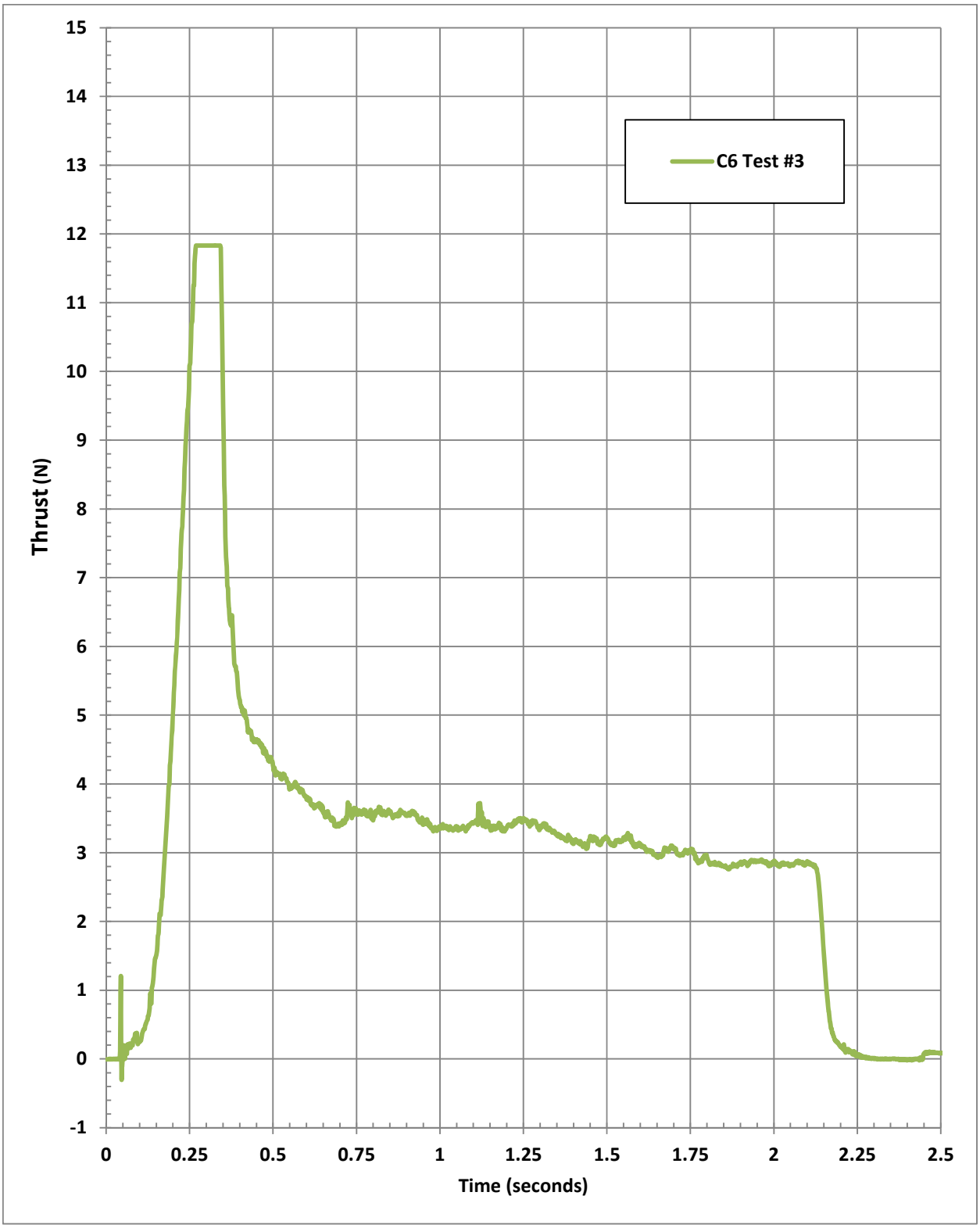

Figure B-3. "C6 Static Test #3".

Note: the peak thrust was clipped due to using the high resolution (0-10 N) setting of the dual range force sensor.

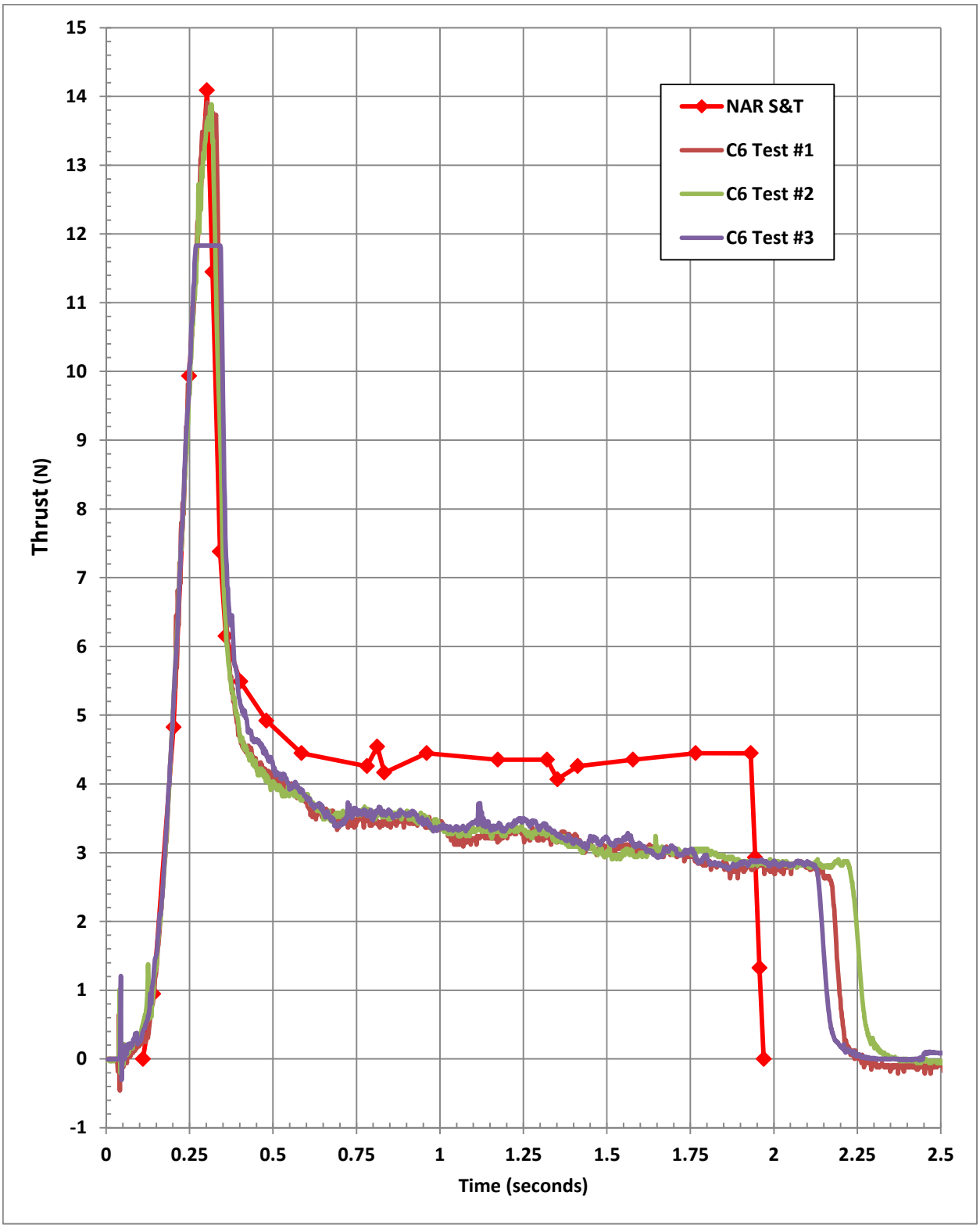

Figure B-4. C6 static tests and NAR S&T data.

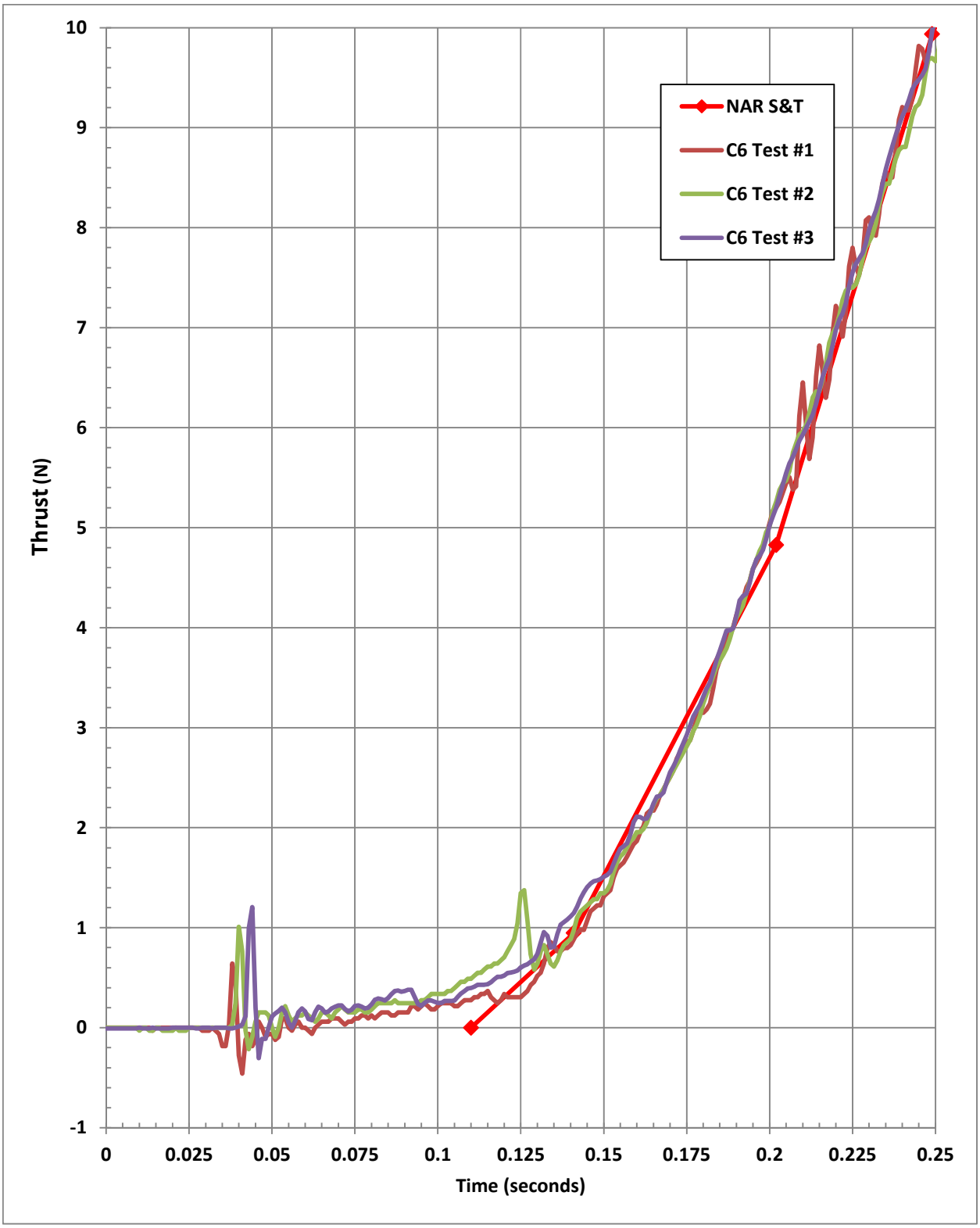

Figure B-5. C6 static tests and NAR S&T data.